energy&fuels

pubs.acs.org/EF

Article

Toward Native Hardwood Lignin Pyrolysis: Insights into Reaction Energetics from Density Functional Theory

Tanzina Azad, Maria L. Auad, Thomas Elder, and Andrew J. Adamczyk*

Cite This: https://doi.org/10.1021/acs.energyfuels.2c03025

Read Online

ACCESS | Metrics & More | Article Recommendations | Supporting Information

ABSTRACT: Lignin is one of the three structural components of lignocellulosic biomass and the only renewable source for sustainably producing aromatic chemicals. Despite lignin's promise for targeted valorization to fine chemicals, fuels, and polymer composites, a major roadblock is an ambiguity associated with its molecular structure. Due to the lack of an established molecular structure, all types of computational studies from reaction mechanism to reaction energetics are performed with model lignin compounds. Among several thermochemical conversion techniques, lignin pyrolysis has been an active research area for both experimental and computational investigations. Historically, computational studies on the pyrolysis of lignin have mainly been limited to dimeric or trimeric models using electronic structure methods. Very recently, model oligomers up to the size of decamers have been studied with density functional theory (DFT) calculations. While these studies used very simplified models to study lignin's pyrolysis behavior, theoretical investigations on a more realistic lignin structure are warranted to advance its state-of-the-art. To address this, we have modeled a native hardwood lignin polymer consisting of 20 repeating units, including all three monolignols, i.e., guaiacyl (G), syringyl (S), and *p*-hydroxy coumaryl (H) units, and multiple types of linkages, i.e., *β*-O-4, 4-O-5, *β*−*β*, and *β*-5. This more realistic molecular model for the wild-type poplar lignin is based on a proposed lignin structure reported in a previous experimental study. The initial stage in lignin pyrolysis involves the homolytic cleavage of *β*-O-4 linkages present in lignin. The activation energy for homolysis of this linkage is considered to be slightly greater than the bond dissociation enthalpy (BDE) required to cleave it. We used a composite method using molecular mechanics-based conformational sampling and quantum mechanically based density functional theory (DFT) calculations to determine the reaction energetics for this reaction, which indicates the activation energy required for the early stage of lignin pyrolysis. In addition, we calculated standard thermodynamic properties for all species, including enthalpy of formation, heat capacity, entropy, and Gibbs free energy of formation as a function of temperature. This study provides the reaction energetics and standard thermodynamic quantities that could be used in kinetic and reactor modeling for biomass conversion. Additionally, these predictions would be particularly helpful in advanced-generation biorefinery, where hardwoods can be used as a potential feedstock. Moreover, the predictions reported in this study will benefit further computational studies and cross-validation with pyrolysis experiments, ultimately contributing to solving the puzzle of the structural ambiguity of lignin.

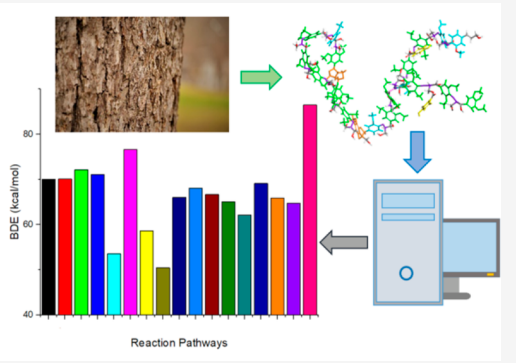

INTRODUCTION

Lignocellulosic biomass is one of the many alternative energy resources but the only sustainable source for producing bio-based chemicals. Biomass valorization is paramount to the concept of a "Biorefinery" based on lignocellulosic feedstock (LCF). A biorefinery is similar to a petroleum refinery except that it uses biomass instead of crude oil as the input and is still in the pilot stage of its development. While existing pulp and paper mills can be considered phase 1 biorefineries, the transition from phase 1 to phase 3 depends on our understanding of the biomass structure and its effective valorization techniques. Lignocellulosic biomass is composed of three biopolymers: cellulose, hemicellulose, and lignin. In the recent past, there have been notable advancements in the fundamental understanding of the overall plant cell wall, characterization, and engineering principles for its diverse and targeted conversion. However, lignin is severely underutilized mainly due to its structural complexity. Due to the lack of a specific monomer and an interunit linkage, lignin should be considered as a generic term for a large group of aromatic polymers resulting from the oxidative combinatorial coupling of 4-hydroxyphenyl propanoids.[1] The task of lignin is to impart rigidity into the plant cell wall, protect against microbial degradation, and participate in water interactions. This

Received: September 13, 2022
Revised: November 17, 2022

biopolymer contributes the most to the overall biomass valorization recalcitrance. Considering this limiting factor in biomass valorization, research efforts have been made to design plants that either deposit less lignin or produce lignin that is more easily degradable.[2−4] The specific role of lignin and the challenges associated with it in the context of biorefinery have been discussed in many recent articles.[5−8]

Although the understanding of lignin composition continues to be refined, three hydroxyl cinnamyl alcohols, coniferyl alcohol, sinapyl alcohol, and *p*-coumaryl alcohol, are established as the primary building blocks for lignin biosynthesis. The units resulting from these monolignols are called guaiacyl (G), syringyl (S), and *p*-hydroxyphenyl (H) units. Various chemical methods, including nitrobenzene oxidation,[9] pyrolysis gas chromatography−mass spectrometry (Py-GC/MS),[10] thioacidolysis,[11] and derivatization followed by reductive cleavage (DFRC)[12] and instrumental methods, mostly NMR, have been used to elucidate lignin's structure.[13−15] According to Ralph et al., the NMR methods cannot deduce the primary structure of lignin with the sequence of H, G, and S units.[13] Furthermore, these methods can only analyze a fraction of the lignin polymer, which emphasizes the necessity for examining the complete composition of lignin in a plant. The ambiguity of the lignin structure is also attributed to the presence of several interunit linkages. In addition to the ubiquitous linkage of *β*-aryl ether, the presence of other linkages, including phenyl coumaran (*β*-5), resinol (*β*−*β*), and biphenyl ether (4-O-5), have been reported.[16,17] According to some recent studies, lignin might be a more homogenous structure than the commonly held assumption that lignin is a highly heterogeneous polymer. Crestini et al. concluded that milled wood lignin, which is structurally most representative of the native lignin, is linear.[18] According to this study, milled wood lignin samples derived from various soft and hardwoods are linear oligomers with the degree of polymerization ranging from 5 to 12. In a very recent study led by Ralph et al.,[17] two possible 20-mer structures have been proposed for gymnosperms and angiosperms, both of which are predominantly linear. The *β*-O-4 content is higher for both of these models (60% in gymnosperm and 80% in angiosperm), whereas the other linkages reported are *β*-5, *β*−*β*, and 4-O-5, spirodieneone and dibenzodioxocin linkages. While this study[17] proposing these two linear structures mentioned that a Y-type branch point might not be formed for native lignin, a small branching resulting from the 4-O-5 linkage has been reported in a study by Stewart et al. representing the structure for native wild-type poplar lignin.[16] The lignin polymer model shown in a study Stewart et al.[16] has a molecular weight of 4514.53 g mol^{-1} and was built based on their prior works.[1,19] The model structure for the native wild-type lignin proposed in a study by Stewart et al. is based on experiments using chemical and analytical analysis of stems collected from 2.5-year-old greenhouse-grown hybrid poplar (*Populus tremula* × *alba*). Considering it to be the most accurate representative structure for hardwood native lignin, we built our molecular model of native lignin based on this reported structure[16] to study its early-stage pyrolysis behavior using computational tools.

Pyrolysis is considered one of the most promising techniques among the thermochemical conversion processes. In pyrolysis, biomass is converted into all three physical states, char (solid), bio-oil (condensable liquid), and noncondensable (gas). Among the different types of pyrolysis, fast pyrolysis is particularly useful for producing bio-oil as it minimizes char formation. Fast pyrolysis of biomass is very interesting because the existing petroleum refinery can work with the bio-oil once processed from the crude biomass.[20] In the context of a third-generation biorefinery, where lignocellulosic biomass would be used as the feedstock, it is crucial to utilize the whole biomass, which demands a clear understanding of all three components' exact composition. Compared to cellulose and hemicellulose, vast information gaps exist for lignin's molecular structure. In practice, it is challenging to study the pyrolysis behavior of native lignin due to the lack of a suitable extraction method that could retain the structural detail of native lignin after its isolation from the lignocellulosic complex. A feasible way to study reaction energetics and mechanism for native lignin pyrolysis is using a computational approach. These aspects of lignin pyrolysis have been studied computationally for the past few decades, resulting in a large and valuable body of literature.[21−29] However, to the best of our knowledge, none of the previous studies have used structures representing the large range of variability in composition and interunit linkages to capture the reaction enthalpies during pyrolysis. There is a lack of a complete representative structure with all monolignols and linkages in a relative ratio that mimics the native lignin in the plant. Furthermore, the computational cost is exceptionally high to study such a large polymer structure, making it difficult to extend the system size beyond dimers. Various linkages important for lignin chemistry have been studied with dimers, trimers, and tetramers,[30] which provided essential quantification of reaction enthalpies for gas-phase pyrolysis of lignin. However, it was beyond the scope of these studies with limited system size to answer whether a range of reaction enthalpies needs to be considered for the initial stages of lignin pyrolysis. Hence, how the lignin polymer chain would behave during pyrolysis with all monomers and linkages warrants investigation.

We considered following the radical mechanism for studying reaction energetics of lignin decomposition, although the existence of a concerted mechanism is also confirmed for lignin pyrolysis. The concerted mechanism for lignin pyrolysis was studied experimentally with phenethyl phenyl ether (PPE) as the model compound reported by Klein and Virk and Jarvis et al.[31,32] In 1983, Klein and Virk conducted the experimental pyrolysis of PPE both in the absence and presence of a hydrogen donor, tetralin at a lower temperature of 300−500 °C in a stainless steel bomb reactor.[31] After finding phenol and styrene as the product, they concluded that the concerted mechanism, i.e., retro-ene and Maccoll elimination mechanisms, best explained their observed results. Later in 2011, Jarvis et al. studied the pyrolysis of PPE using a hyperthermal nozzle with photoionization mass spectroscopy (PIMS) over a wide range of temperatures (300−1350 °C) to determine the importance of both concerted and radical mechanisms for its decomposition pathway.[32] Based on the observed products and theoretical calculations for kinetic parameters of reactions following both mechanisms, this study concluded that the most favorable reaction for PPE decomposition is the retro-ene mechanism at 400 °C, whereas at a temperature greater than 1200 °C, C−O homolysis becomes more favorable. These findings do not support the assumption that the initial stage of lignin pyrolysis starts with the cleaving of the *β*-O-4 bond at the primary pyrolysis stages at 300−400 °C. However, several other reports provide insights that suggest otherwise. Britt et al. studied the pyrolysis of PPE using a constant volume reactor at

https://doi.org/10.1021/acs.energyfuels.2c03025
Energy Fuels XXXX, XXX, XXX−XXX

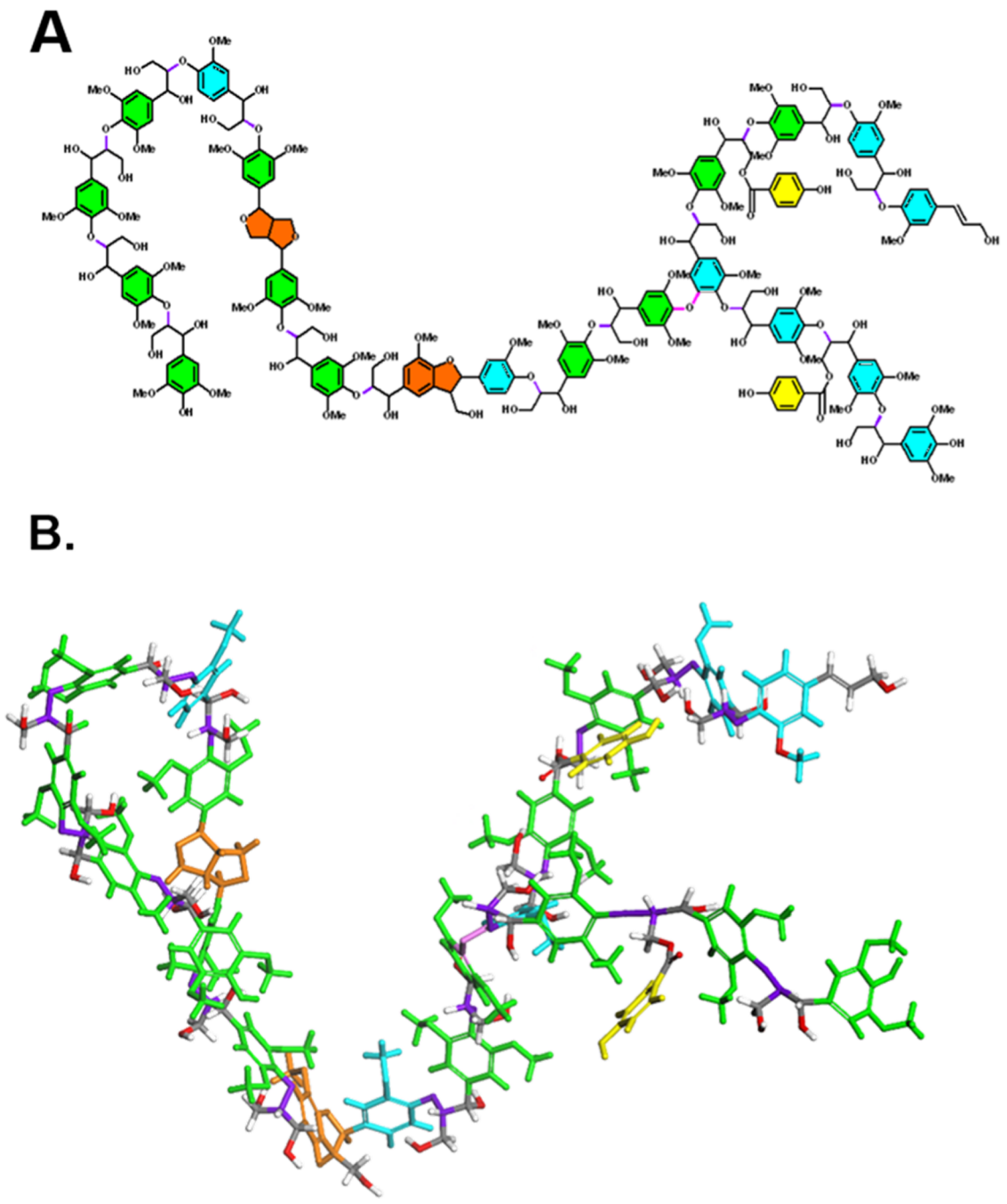

Figure 1. (A) Molecular structure for the 20-mer native poplar lignin taken from a study by Stewart et al.[16] and (B) the molecular model for the same structure. In both figures, different colors have been used to distinguish among the monomers: green: syringyl unit (S), blue: guaiacyl (G), and yellow: p-hydroxy benzoate derived from the *p*-hydroxyphenyl unit (H). Different colors have also been used to differentiate among the linkages: purple: β-O-4, pink: 4-O-5, and orange: β–β and β-5.

330−425 °C for 5−40 min in the liquid phase and 5−480 min in the gas phase.[33,34] They observed the formation of styrene and phenol as the pyrolysis products from PPE but concluded that phenol forms from the phenoxy radical. According to this study, homolysis of C−O is the dominant mechanism for PPE decomposition at lower temperatures. Furthermore, lower temperature homolysis of the β-O-4 bond via a quinone methide intermediate has been proposed under different experimental conditions.[35−37] To date, no study has confirmed that the radical mechanism does not occur in the initial stage of lignin pyrolysis. Moreover, the volume of reaction energetics studies employing electronic structure calculations for the radical mechanism is much larger compared to the concerted mechanism. This work focused on the homolysis of β-O-4 so that a comparison can be made with the existing extensive literature.

We applied contemporary computational methods to answer this question to predict the reaction enthalpies associated with a wild-type poplar lignin polymer structure under gas-phase pyrolysis conditions. Our previous works with electronic structure methods investigated two oligomeric model structures for softwood and hardwood lignin, consisting of 10 G and 10 S units connected through nine β-O-4 linkages. We identified marked position dependence of reaction

https://doi.org/10.1021/acs.energyfuels.2c03025
Energy Fuels XXXX, XXX, XXX−XXX

enthalpies on the bond-cleaving positions in these oligomers.[38,39] In the current study, we aim to quantify the range of reaction enthalpies for the homolytic cleavage of the β-O-4 bonds with a focus on the effect of multiple linkages and monomers present in this more realistic lignin model. Given such enormous flexibility, classical molecular mechanics-based conformational sampling, developed in our previous study,[38] has been applied to generate lower energy conformational isomers for the reactant molecule. Afterward, the lowest energy conformer for the reactant was used to generate free radical product species and determine the bond dissociation enthalpies employing density functional theory (DFT). Finally, standard thermochemical properties, including enthalpy, entropy, free energy, and constant pressure heat capacity values, were theoretically estimated using statistical thermodynamics. Although we have studied simplified and idealized model structures in our previous works, the model structure used in the current work depicts the structural features of poplar lignin. It is noteworthy that this is beyond the scope of any model structure to capture all features of this highly complex polymer. We worked with a model structure that has been built on the experimental evidence and accommodates the main linkage types and their approximate relative frequencies. Therefore, we chose this structure as our model for the native hardwood lignin to provide a range of reaction enthalpies for the initial pyrolysis process. Additionally, the predicted range and values for the thermodynamic properties in this study would be beneficial in the detailed kinetic modeling, reactor, and process modeling for lignin valorization.

COMPUTATIONAL METHODOLOGY

Model Generation. Figure 1 represents the model lignin polymer for the wild-type hybrid poplar, which was published in a lignin structure analysis by Stewart et al.[16] The model is based on NMR analysis, coupled with the other analytical and chemical methods, including the Klason lignin content, thioacidolysis, degradative fraction of reductive cleavage (DFRC), methoxyl and hydroxyl content analysis, and HPLC analysis. Table 1 lists the major structural units and linkages with the relative percentages of this model lignin polymer.

Table 1. Major Features of the Model Polymer for Native Wild-Type Poplar Lignin ($C_{228}H_{270}O_{94}$) Taken from a study by Stewart et al.[16]

feature(s)	notation(s)	name(s)	relative amount (%)
monomer	S	syringyl	63.63
	G	guaiacyl	27.27
	SP	sinapyl *p*-hydroxy benzoate	9.1
linkage	β-O-4	β-aryl ether	84.21
	β-5	phenyl coumaran	5.26
	β-β	resinol	5.26
	4-O-5	biphenyl ether	5.26

With 14 S and 6 G units, this model lignin structure has roughly an S/G ratio of 2, which is usual for angiosperms. Since this is a model for hardwood lignin, the frequency of β-O-4 linkage is prevalent in this structure (i.e., ~84.21%). According to Adler,[40] biphenyl ether linkage constitutes 5% of the linkages in the angiosperms; therefore, one 4-O-5 linkage has been included in this model. There are two ester groups, i.e., *p*-hydroxybenzoates, in this proposed structure, accounting for ~10% of the monomers. Both of these groups are connected with two S units on each side and located near the tail of the polymer chain. One phenyl coumaran (β-5) and one resinol (β–β) unit can be seen, while spirodieneone (β-1) and dibenzodioxocin units are not present in this structure. The proportion of cinnamyl alcohol end-groups is relatively minor, which arises from the monomer–monomer coupling. Only one such group is present in this structure.

It is noteworthy that it is beyond the scope of any model to portray the native lignin structure entirely and capture its H/G/S sequences accurately. Also, this is only one of many possible lignin isomers.[41] This model lignin polymer accommodates the dominating linkage types while maintaining their relative frequencies using evidence derived from the experiments. Therefore, we have used this proposed structure to generate our molecular model for the lignin polymer, as shown in (Figure 1B), to better understand the primary pyrolysis response of native hardwood lignin model polymer.

Reaction Pathway Schemes. The reactions examined in this work are shown in Table 2, representing the successive homolytic cleavage of 16 β-O-4 bonds and one bond arising from the homolytic cleavage of the 4-O-5 bond, denoted by B_i (i = 1–16) and A_j (j = 1), respectively. For all of the pathways, the homolytic cleavage of β-O-4 bonds resulted in two radical products: one phenoxy and one carbon-centered radical species. The homolytic cleavage of the 4-O-5 bond resulted in one phenoxy radical and one phenyl radical species. We studied this linkage along with the β-O-4 bonds in this system since it is an ether linkage too. With an S/G ratio of 2 and the inclusion of diverse monomers and linkages, the model shown in Figure 1A represents a realistic native lignin structure. In our previous work, we used more idealized structures than the current model to test our hypothesis that the BDE values depend on the bond position being cleaved along the model oligomer chain. Hence, sequential cleavage of β-O-4 bonds in those two models resulted in relatively straightforward reaction schemes, differing only in the chain length of oligomeric product species. Due to using a more realistic native lignin model, the reaction scheme followed in this work generated radical product species for which the polymer chain length did not increase successively. For pathways B_1–B_5 and B_{10}–B_{12}, the molecular weights of the phenoxy species were significantly higher than the carbon-free radical species. In contrast, the opposite trend has been found for the pathways B_{13}–B_{16}, where the carbon-free radicals were the larger products. Products with roughly similar atom numbers have been observed for the pathways from B_6 to B_9 and A_1, for the β-O-4 and 4-O-5 linkages, respectively.

Conformational Analysis. In this work, a conformational sampling method developed in our previous study[38] was used with modification to generate the lowest energy conformer for the reactant molecule, i.e., the 20-mer wild-type hardwood lignin model. We used COMPASS[42] (Condensed-phase optimized molecular potentials for atomistic simulation studies) with its forcefield assigned charges to locate the local energy minimum of the closed shell reactant molecule along its potential energy surface. Next, the conformational search was stochastically performed employing the Boltzmann jump method. In the Boltzmann jump, the number of perturbation steps to be carried out for each jump cycle was selected as 50, and a sampling temperature of 5×10^4 K was used for the search. Among all of the bonds capable of rotation

https://doi.org/10.1021/acs.energyfuels.2c03025
Energy Fuels XXXX, XXX, XXX–XXX

Table 2. Chemical Structures of Radical Products Obtained Along Each Reaction Pathway for Studying the BDEs of the Selected Linkages in This Work[a]

Reaction Pathway	Product 1 (Phenoxy radical species)	Product 2 (Carbon free radical species)
B_1	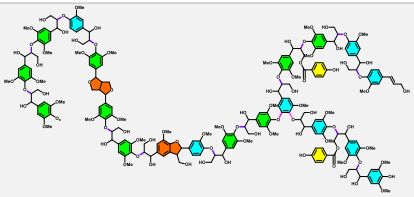	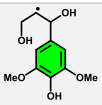
B_2	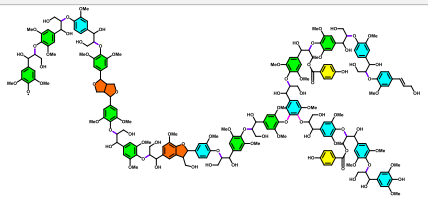	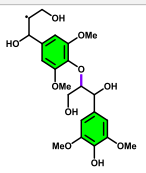
B_3	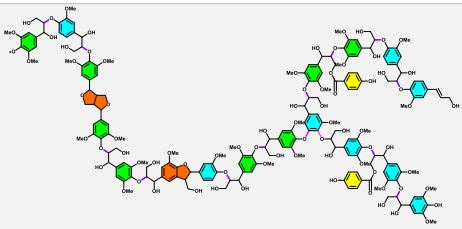	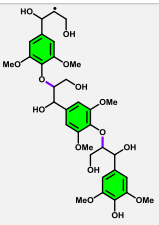
B_4	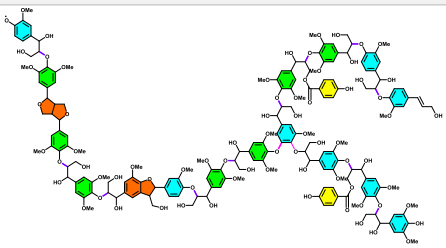	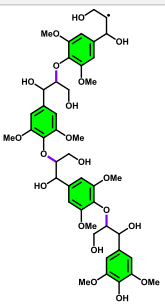
B_5	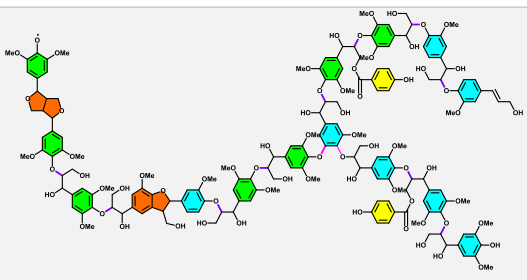	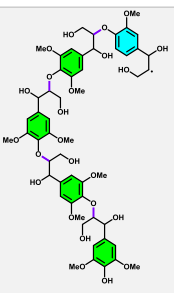
B_6	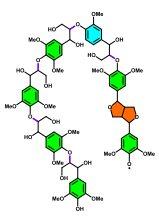	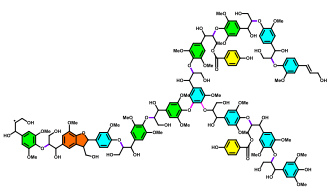

https://doi.org/10.1021/acs.energyfuels.2c03025
Energy Fuels XXXX, XXX, XXX−XXX

Table 2. continued

Reaction Pathway	Product 1 (Phenoxy radical species)	Product 2 (Carbon free radical species)
B_7	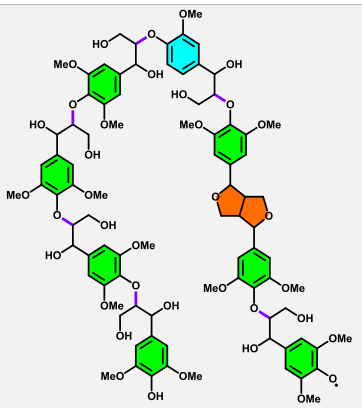	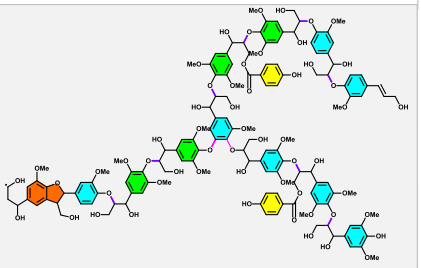
B_8	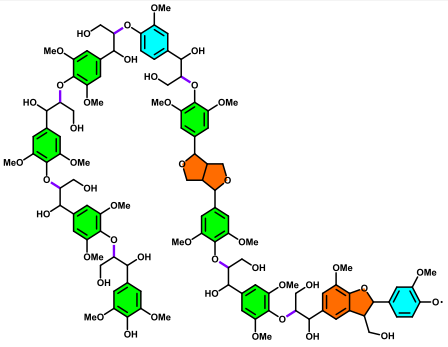	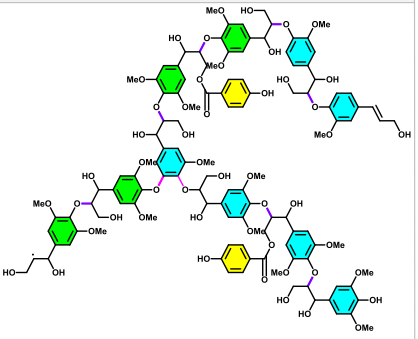
B_9	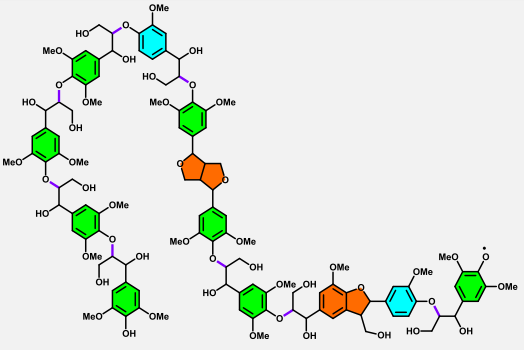	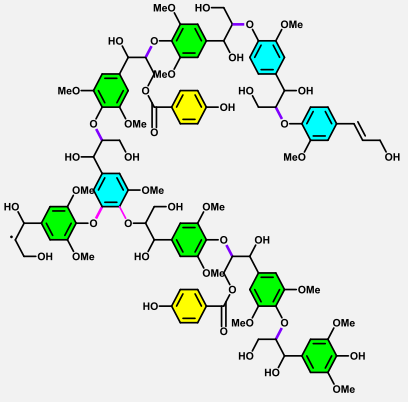
B_{10}	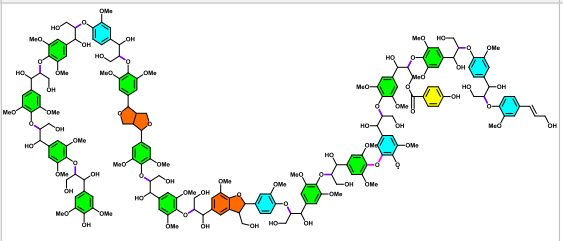	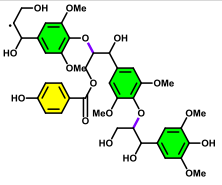

https://doi.org/10.1021/acs.energyfuels.2c03025
Energy Fuels XXXX, XXX, XXX−XXX

Table 2. continued

Reaction Pathway	Product 1 (Phenoxy radical species)	Product 2 (Carbon free radical species)
B_{11}	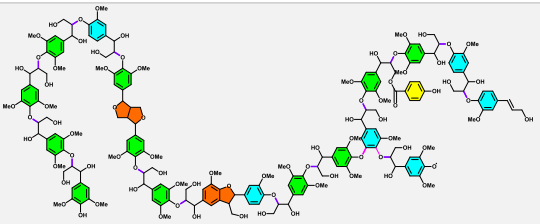	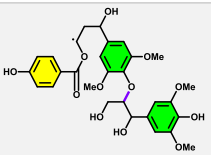
B_{12}	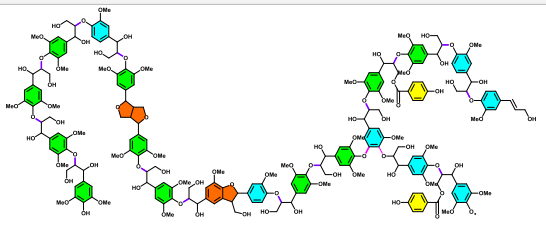	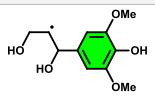
B_{13}	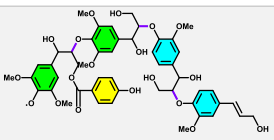	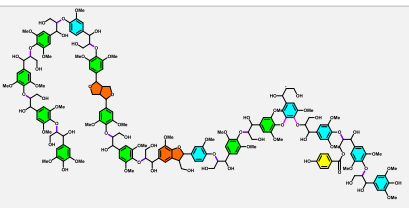
B_{14}	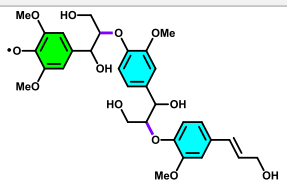	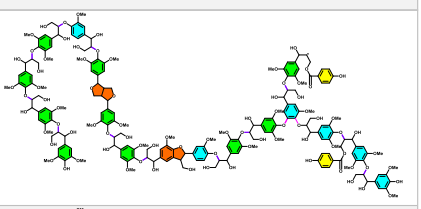
B_{15}	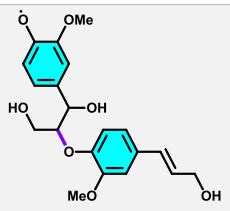	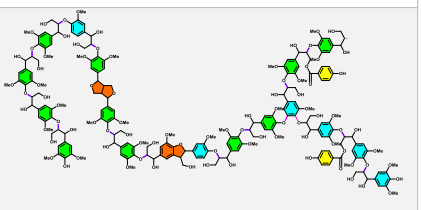
B_{16}	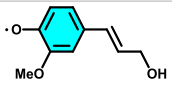	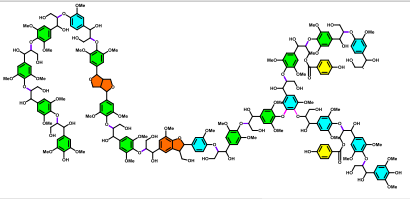
A_1	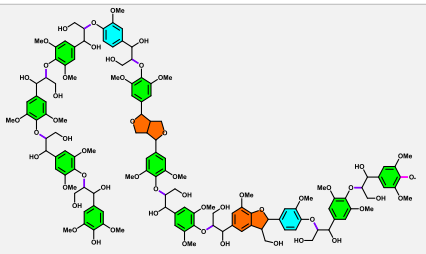	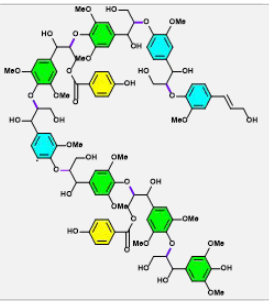

[a]Pathways B_1−B_{16} denote β-O-4 linkages, and A_1 implies 4-O-5 linkage.

along about any σ bond, 128 randomly selected dihedral angles were altered within a specified angular window of 10°. The Metropolis selection criterion was employed after each of these random moves. After a random move, if the change in energy (ΔE) is negative, the move is accepted. If ΔE is positive, the Boltzmann factor, $F = \exp^{(-\Delta E)/RT}$, is computed and a random

https://doi.org/10.1021/acs.energyfuels.2c03025
Energy Fuels XXXX, XXX, XXX−XXX

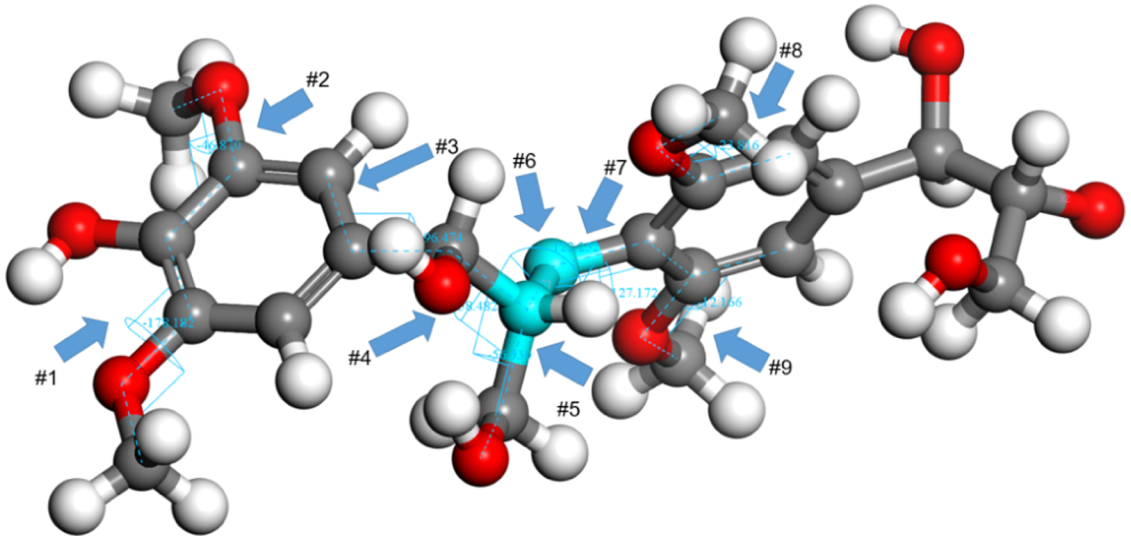

Figure 2. Representative torsion angles that were altered randomly within the allowed angular window of 10° in the used conformational sampling method. A total of 128 dihedral angles were varied to reach the lowest energy conformers for the macromolecule being analyzed here. For clarity, only the first 9 among all 128 dihedral angles that fell within the first two syringyl units linked by the first β-O-4 bond (labeled in light blue color) have been shown in this figure. The optimized dihedral angles for these nine parameters are: C−C−O−C (1): −178.18°, C−C−O−C (2): −46.87°, C−C−C−C (3): −96.47°, C−C−C−C (4): −58.48°, C−C−C−O (5): −56.53°, C−C−O−C (6): 122.25°, C−O−C−C (7): 127.17°, C−C−O−C (8): −23.82°, C−C−O−C (9): −12.17°.

number from 0 to 1 is generated. If the random number is less than the calculated F, the move is accepted according to the Metropolis selection criterion.[43] Each conformer search step generated 1000 conformers, from which the conformer with the lowest total optimized energy was selected as the input for the next search. The Smart optimization algorithm was used during conformational sampling, where the convergence tolerances were 0.001 kcal mol^{-1} for energy, 0.5 kcal mol^{-1} Å^{-1} for force, and 0.015 Å for displacement. The Smart algorithm is a cascade of the steepest descent, ABNR (adjusted basis set Newton−Raphson), and quasi-Newton methods. This iterative process of conformer searching was continued until no statistically significant variance was found in the total energy value for the conformer identified with the COMPASS forcefield. Atom-based electrostatics and van der Waals (vdW) summation methods were used for considering the nonbonded options and performed with cubic spline truncation, employing a cut-off distance of 12.5 Å, a spline width of 1 Å, and a buffer width of 0.5 Å.

Electronic Structure Calculations. The electronic energies for all structures were calculated using DFT in the Dmol3 package considering all electrons for each atom using the BLYP density functional.[44] A numerical basis set of double zeta quality plus polarization functions (DNP) was used, which allowed for the truncation of the numerical integration, thus increasing the computational efficiency. We selected the BLYP/DNP level of theory after assessing its performance in studying reaction energetics and predicting thermochemistry for lignin model oligomeric species in our previous two studies[38,39] as well as the reported use of BLYP/DNP for studying organic compounds with similar objectives.[45−48] The Tkatchenko−Scheffler (TS) method was used as the dispersion correction to include nonbonded interactions.[49] Using the lowest energy conformation for the reactant, geometry optimization was done at the BLYP/DNP level where the convergence tolerances were 2× 10^{-5} Hartree for the total energy, 0.004 Ha/Å for the maximum force, and 0.005 Å for the maximum displacement. All electrons were chosen as the core treatment with an orbital cut-off scheme of global with the orbital cut-off energy 4.4 Å. For the SCF cycle, the tolerance used was 1× 10^{-5}, with a maximum SCF cycle set at 1000. We used a DIIS of size 6 and the multipolar expansion of hexadecapole. A charge of 0.2 and a spin of 0.5 were used as the density mixing in this work. All calculations were done at the gas phase.

After geometry optimization at the BLYP/DNP level, calculated vibrational frequency calculations, along with the calculated equilibrium geometries, were used to yield a variety of thermodynamic quantities at the same level of theory. The values for enthalpy (H), entropy (S), free energy (G), and heat capacity at constant pressure (C_p) as functions of temperature were obtained from standard statistical thermodynamics using molecular partition functions based on the harmonic oscillator and rigid rotor approximations for polyatomic gas molecules.[50] Details on the calculation of these properties, including the electronic, translational, rotational, and vibrational contributions for the molecular partition functions, can be found in the Supporting Information. Small inorganic systems with objectives of studying the reactive features similar to this work have been extensively studied with success in our group using comparable hybrid methodologies.[51−63] The radical product geometries were based on the geometry of the low energy conformation of the reactant, with the appropriate bonds cleaved, followed by optimization using the electronic structure methods previously described but without conformational searching. This approach has been used in previous works[64,65] to find the nearest local minimum while avoiding large-scale changes that could occur with a conformational search.

Bond Dissociation Enthalpies. We employed the values of standard enthalpies of formation from the statistical thermodynamics calculations to calculate BDEs. BDEs were calculated at the reference temperature as the difference of the sum of the standard enthalpies of formation of the product

https://doi.org/10.1021/acs.energyfuels.2c03025
Energy Fuels XXXX, XXX, XXX−XXX

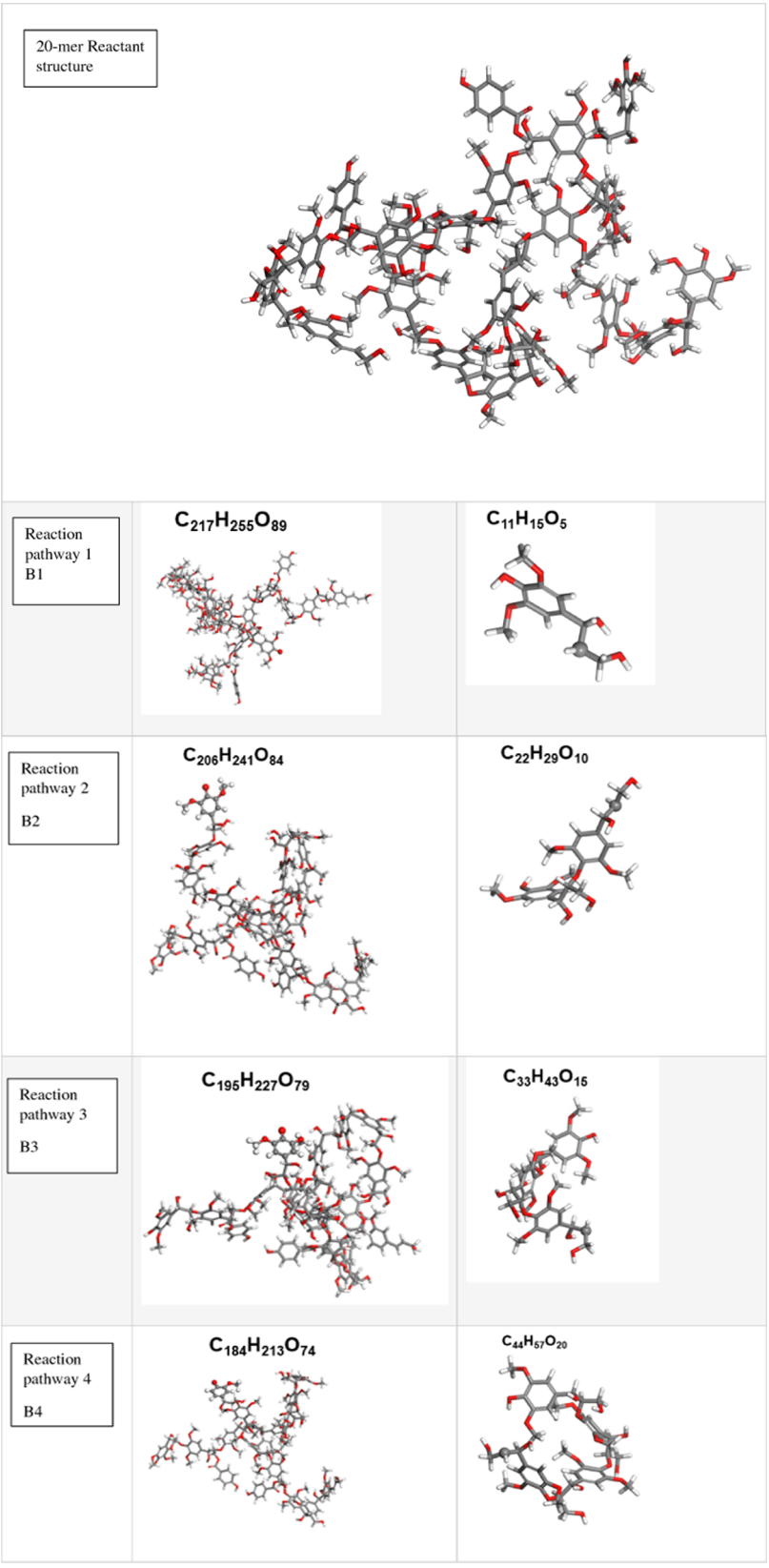

Figure 3. continued

https://doi.org/10.1021/acs.energyfuels.2c03025
Energy Fuels XXXX, XXX, XXX−XXX

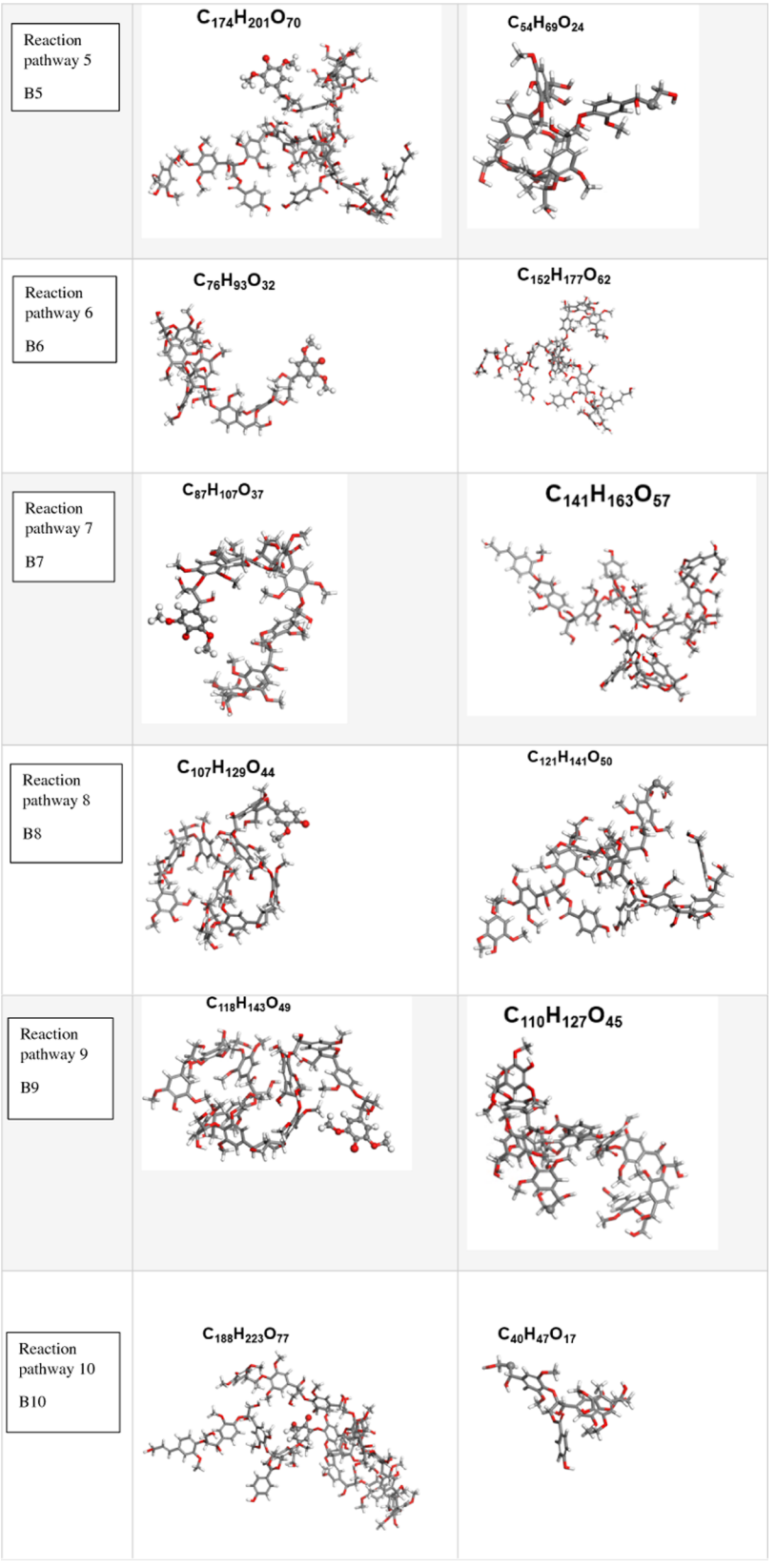

Figure 3. continued

https://doi.org/10.1021/acs.energyfuels.2c03025
Energy Fuels XXXX, XXX, XXX−XXX

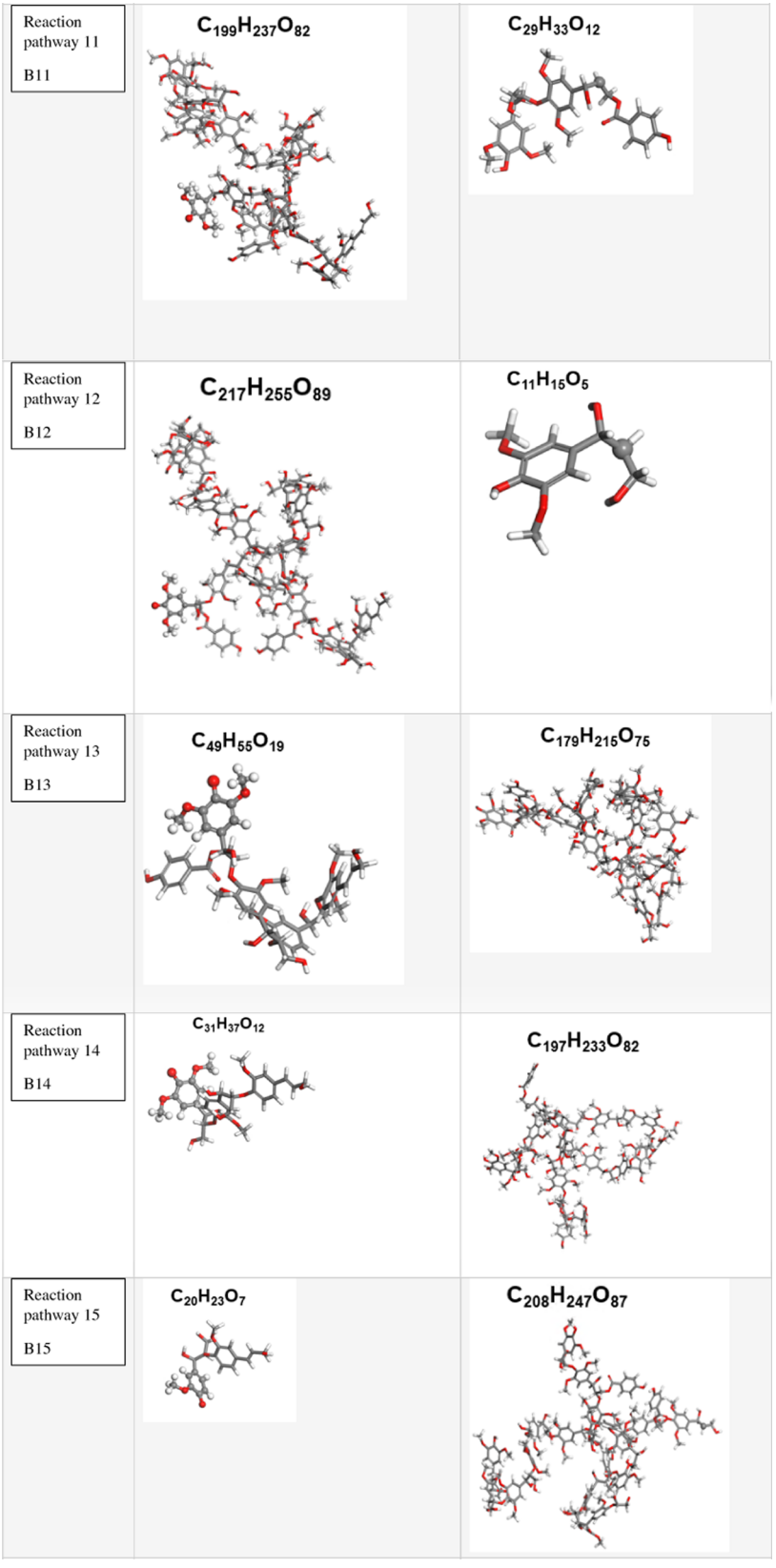

Figure 3. continued

https://doi.org/10.1021/acs.energyfuels.2c03025
Energy Fuels XXXX, XXX, XXX−XXX

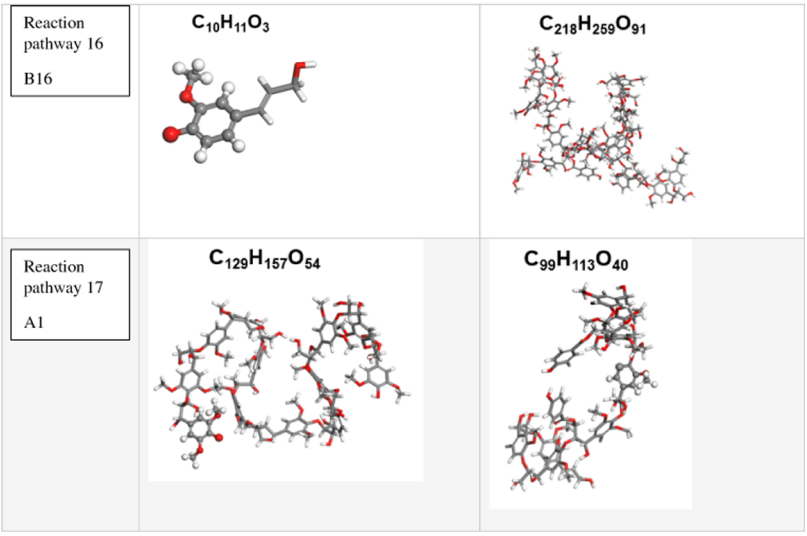

Figure 3. Optimized structures for all products and the reactant at the BLYP/DNP level of theory for this study.

fragments and the standard enthalpy of formation of the reactant, as shown in eq 1

$$\mathrm{BDE}_{298\ (\text{reaction pathway})} = [\Delta H^{\circ}_{f,298\ (\text{product 1})} + \Delta H^{\circ}_{f,298\ (\text{product 2})}] - \Delta H^{\circ}_{f,298\ (\text{reactant})} \quad (1)$$

where $\Delta H^{\circ}_{f,298}$ is the standard enthalpy of formation of the radical species Products 1 and 2, and the reactant is the native model lignin 20-mer. Following the hybrid methodology used in the previous work from our group,[51] we computed the enthalpy of formation values for all species combining quantum chemical calculations, statistical thermodynamics, and experimental values for atomization energies. The enthalpy of reaction at elevated temperature, i.e., BDE at temperature T, can be calculated using the calculated $\mathrm{BDE}_{298\ \mathrm{K}}$ and temperature-dependent heat capacity values using eq 2

$$\mathrm{BDE}_T = \mathrm{BDE}_{298\ \mathrm{K}} + \int_{298\ \mathrm{K}}^{T} \Delta C_{p,\mathrm{Rxn}}(T)\, \mathrm{d}T \quad (2)$$

where $\Delta C_{p,\mathrm{Rxn}}(T)$ is the temperature-dependent polynomial defined as the difference between the sum of the temperature-dependent standard heat capacities of the products and the temperature-dependent standard heat capacity of the reactant.

RESULTS AND DISCUSSION

Model Selection. Studies on the structural aspects of different types of lignin have refined the overall knowledge of its structure, which continues to be expanded using both experimental and computational tools. Understanding the native lignin structure has been significantly advanced by the insights from structural studies with transgenic lignin. The model we selected for this study comes from an experimental investigation[16] that proposed and compared two molecular structures, wild-type hybrid poplar and transgenic lignin, created by upregulation of C4H::F5H in the plant, respectively. Due to the overexpression of the F5H enzyme in the transgenic plant, it exists as a fully linear model, while the native poplar lignin model has one branch point arising from the 4-O-5 linkage present in this structure. A molecular structure for angiosperm/dicot lignin has been proposed in a recent study by Ralph et al.,[17] which is also a 20-mer structure and has one 4-O-5 linkage; however, the proposed structure does not contain a Y-type branch point, unlike our selected model in this study. Apart from this dissimilarity, the other features, namely, the presence of one phenyl coumaran (β-5), one resinol unit ($\beta-\beta$), and the absence of spirodienone and dibenzodioxocin units, are similar in both of these two hardwood model lignin 20-mer structures. Dibenzodioxocins are 8-membered ring structures that result from the radical coupling of a monolignol with a 5−5 coupled end unit[66] and are most prevalent in gymnosperms.[67] Another linkage, α-aryl ether, which has been extensively studied in low molecular weight synthetic and model lignin compounds, is not present in our selected model lignin structure because sufficient pieces of evidence are not available for the α-aryl ether linkage to be present in the plants.[68] The frequency of β-O-4 linkages in our selected native model for poplar lignin is similar to that of the native model for angiosperm lignin[17] (i.e., 16 β-O-4 linkages accounting for ~80% of the total linkages).

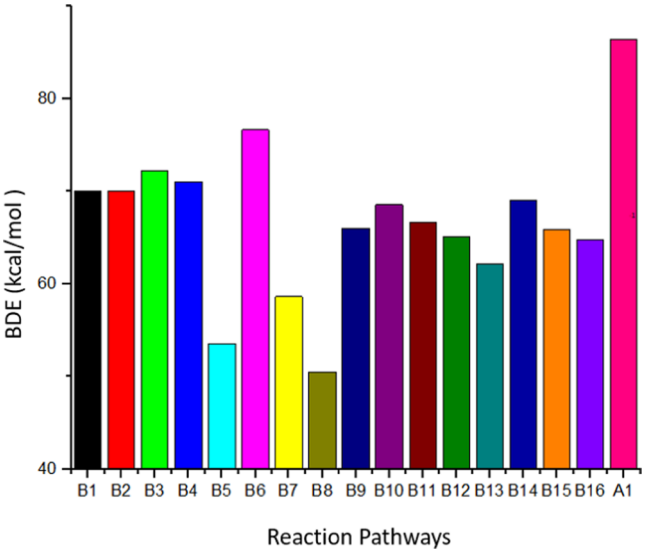

Figure 4. BDE values for the homolytic cleavage of the β-O-4 reaction in the native model lignin polymer at different bond-cleaving positions at 298.15 K.

https://doi.org/10.1021/acs.energyfuels.2c03025
Energy Fuels XXXX, XXX, XXX−XXX

Table 3. Effect of Neighboring Groups on the Calculated BDE at 298.15 K

Reaction Pathway	BDE at the reference temperature (kcal mol^{-1})	Neighboring groups	Cleaved bond
B_1	70.00	S-S	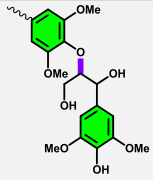
B_2	70.06	S-S	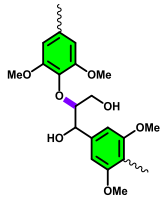
B_3	72.16	S-S	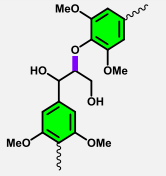
B_4	71.04	S-G	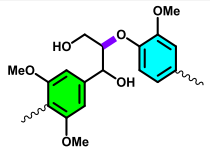
B_5	53.54	G-S	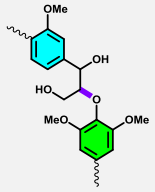
B_6	76.65	S-S	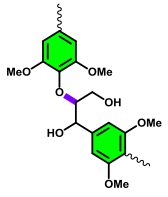
B_7	58.60	S-G	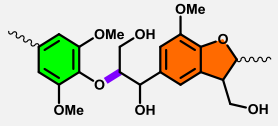
B_8	50.46	G-S	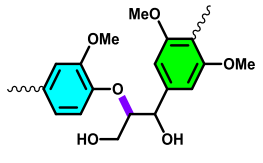

https://doi.org/10.1021/acs.energyfuels.2c03025
Energy Fuels XXXX, XXX, XXX−XXX

Table 3. continued

Reaction Pathway	BDE at the reference temperature (kcal mol^{-1})	Neighboring groups	Cleaved bond
B_9	66.01	S-S	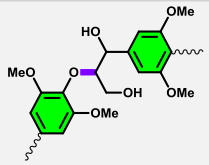
B_{10}	68.09	G-S	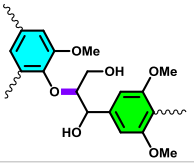
B_{11}	66.63	S-S	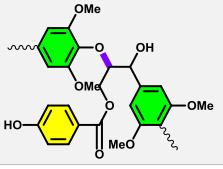
B_{12}	65.07	S-S	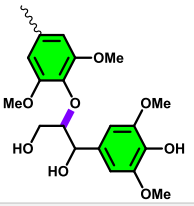
B_{13}	62.13	G-S	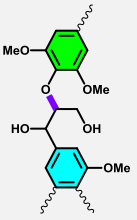
B_{14}	69.08	S-S	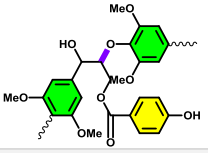
B_{15}	65.84	S-G	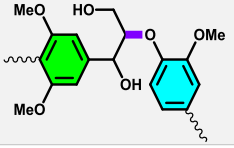
B_{16}	64.73	G-G	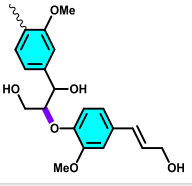
A_1	86.44	S-G	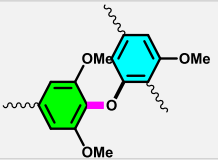

Using electronic structure calculations in our selected molecular model, we provided novel insights into the pyrolysis behavior of native hardwood lignin. This novel insight might be helpful as a starting point for further studies, which are required to make a more generalized conclusion. For example, we studied only one linkage order in our model, which was proposed in a study by Stewart et al.[16] Additionally, since the results from geometry optimization and vibrational frequency

https://doi.org/10.1021/acs.energyfuels.2c03025
Energy Fuels XXXX, XXX, XXX−XXX

Table 4. Comparison of the Computed BDE Along Each Pathway at the Reference Temperature in This Study with the Contemporary Theoretical Studies

reaction pathway	BDE at the reference temperature (kcal mol^{-1})	neighboring groups	Kim et al.[23]	% deviation from this study	Parthasarathi et al.[22]	% deviation from this study
B_1	70.00	S−S	70.50	0.714	NA	NA
B_2	70.06	S−S	70.50	0.63	NA	NA
B_3	72.16	S−S	70.50	−2.30	NA	NA
B_4	71.04	S−G	71.80	1.07	NA	NA
B_5	53.54	G−S	68.20	27.38	64.61	20.68
B_6	76.65	S−S	70.50	−8.02	NA	NA
B_7	58.60	S−G	71.80	22.53	NA	NA
B_8	50.46	G−S	68.20	35.16	64.61	28.04
B_9	66.01	S−S	70.50	6.80	NA	NA
B_{10}	68.09	G−S	68.20	0.16	64.61	−5.11
B_{11}	66.63	S−S	70.50	5.81	NA	NA
B_{12}	65.07	S−S	70.50	8.34	NA	NA
B_{13}	62.13	G−S	68.20	9.77	64.61	3.99
B_{14}	69.08	S−S	70.50	2.06	NA	NA
B_{15}	65.84	S−G	71.80	9.05	NA	NA
B_{16}	64.73	G−G	69.20	6.91	67.33	4.02
A_1	86.44	S−G	71.80	−16.94	82.54	− 4.51

calculations depend strongly on the final conformation of the model, it is never possible to reach a conclusive decision after studying only one model. However, the computational cost for studying this single model was found to be several weeks, a significant limitation for carrying out our further electronic structure calculations of such larger models. Therefore, to balance the necessity of concluding and the significantly higher computational cost, we recommend studying multiple 20-mer lignin models and applying machine learning methods after altering the linkage order within a 20-mer lignin chain.

Conformational Analysis. Conformational analysis is an essential step to identify the lowest energy conformer for any chemical species before performing any quantum mechanical calculation to predict chemical properties. The lignin model we generated for this work is a 592-atom structure, which has several functional groups, including 20 6-membered rings with varying contents of substituent groups. The substituents for these phenyl rings included −OH, $-OCH_3$, and −COOR groups, among which the −OH and $-OCH_3$ are electron-donating and the −COOR is the electron-withdrawing group. In addition to these substituents, the 16 β-O-4 and one 4-O-5 bonds, both ether linkages, are also electron-donating groups. In contrast to cellulose, lignin has an immensely variable structure where the role of these different substituents should be studied carefully. Hence, a large conformational space for this large model lignin polymer has been generated and studied in this work.

We considered the Boltzmann jump search to examine the lignin macromolecule owing to its large number of variable torsions. The systematic grid scan method would produce an unmanageable number of conformers though it could ensure reaching the global minima for this macromolecule. Since this work aimed at using conformational sampling to obtain improved input geometries for DFT calculations, the local minimum energy identified from this sampling served the purpose. Variables that influenced the performance of this Boltzmann jump-based conformation search included torsional angles and sampling temperatures. The magnitude of the conformational change is determined by the width of the torsion angle window during a single perturbation. While a larger window increases the chances of producing higher energy conformers, thereby increasing the chance of rejection in the Metropolis criterion, a narrow window for torsional angle variation increases the chance of acceptance. However, using a narrow window also necessitates using a large number of perturbations to develop an appreciable root mean square difference from the initial conformation. To balance between these two effects, we used the values of 10 and 50 for the allowed angular window and the number of perturbations per jump, respectively, which we found as the optimum values for our system and conformational sampling method. Figure 2 shows a representative structure, which is truncated from the 20-mer structure into a dimer for visualizing which dihedral angles were randomly altered in this work.

In addition to the torsional angle variable, we found the effect of sampling temperature as critical for the Boltzmann jump. At higher temperatures, larger increases in energy are more likely to be accepted. While this increased chance of accepting high-energy conformers is undesirable, using high energy also increases the chance of locating new energy minima. For the large and flexible model that we studied in this work, we found that a simulation temperature of 6×10^5 K was optimal to generate 1000 conformers in each jump. The average total optimized energy obtained during a conformational search step generating 1000 conformers was 551 kcal mol^{-1}. Because of this high temperature, we observed a very large variance of 2299.11 kcal mol^{-1} in these optimized total energy values. At the same time, using such a higher simulation temperature allowed for the generation of a local minimum with 389.11 kcal mol^{-1}, which was significantly lower than the conformer with an optimized total energy of 671.65 kcal mol^{-1}, i.e., the highest energy conformer among the 1000s.

Figure 3 shows the lowest energy conformer identified for the reactant molecule using our conformational sampling method and the two types of product radicals obtained from this reactant conformer. In this work, we employed a modified approach to our previously developed conformational sampling.[38] Using this, the modified approach was prompted because of the sharp increase in the system size in the current work. In our previous works with model lignin decamers

https://doi.org/10.1021/acs.energyfuels.2c03025
Energy Fuels XXXX, XXX, XXX−XXX

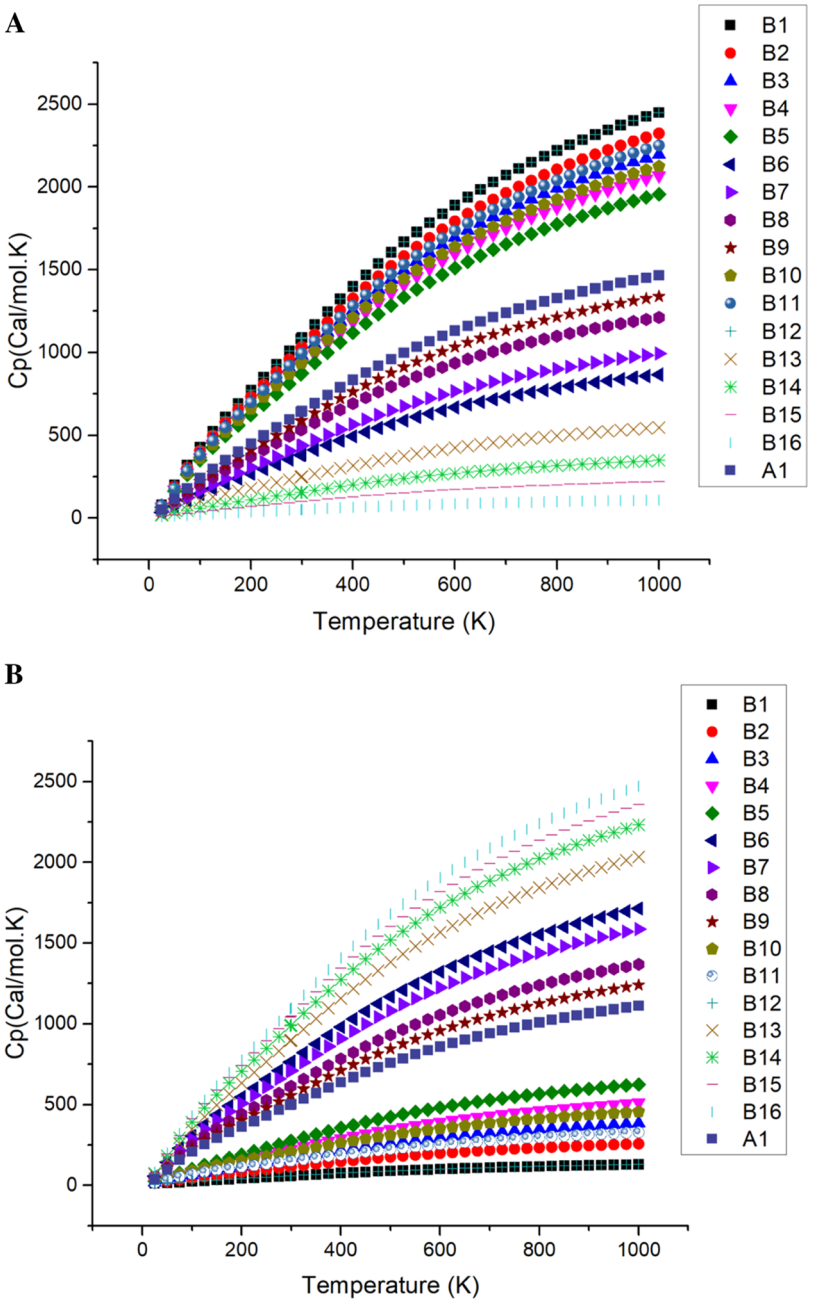

Figure 5. (A) Constant Pressure heat capacities of product 1 species. (B) Constant Pressure heat capacities of product 2 species.

Table 5. Comparison of Predicted C_p Values at Selected Temperatures with Other Works[a]

type of lignin	reference(s)	@ 298 K	@ 350 K	@ 450 K
cuprammonium[b]	Voitkevich et al.[75]	1.24	1.42	NA
sulfuric[b]	Voitkevich et al.[75]	1.28	1.47	NA
dioxane[b]	Hatakeyama et al.[76]	NA	1.21	1.95
softwood model[c]	Azad et al.[38]	1.05	1.21	1.51
hardwood model[c]	Azad et al.[39]	1.10	1.26	1.55
native hardwood[c]	this study	1.02	1.22	1.50

[a]Unit of C_p is in J g^{-1} K^{-1}. [b]Experimental studies. [c]Computational studies.

consisting of only nine β-O-4 linkages, we performed conformational sampling after cleaving each of the bonds after the model oligomer generation using the Lignin Builder algorithm.[69] The model used in the current study includes 16 such β-O-4 linkages and irregular placement of the H, G, and S units as the monomers. Since we studied a 20-mer structure in this work, at first, we determined the lowest energy conformer for the reactant molecule. Then, we cleaved the selected linkages homolytically to obtain the radical products. Performing a conformational search on each of the product radicals could result in misrepresentation of the bond strength, such that the conformational search was only performed on the reactant structure, as has been used in other DFT studies.[64,65,70,71]

Using a 20-mer structure as the input for our conformational sampling method resulted in different criteria as the descriptors of the lowest energy conformer. In our previous works, we used the end-to-end distance as the descriptor of the local energy minimum for all species. This was possible because, in

https://doi.org/10.1021/acs.energyfuels.2c03025
Energy Fuels XXXX, XXX, XXX−XXX

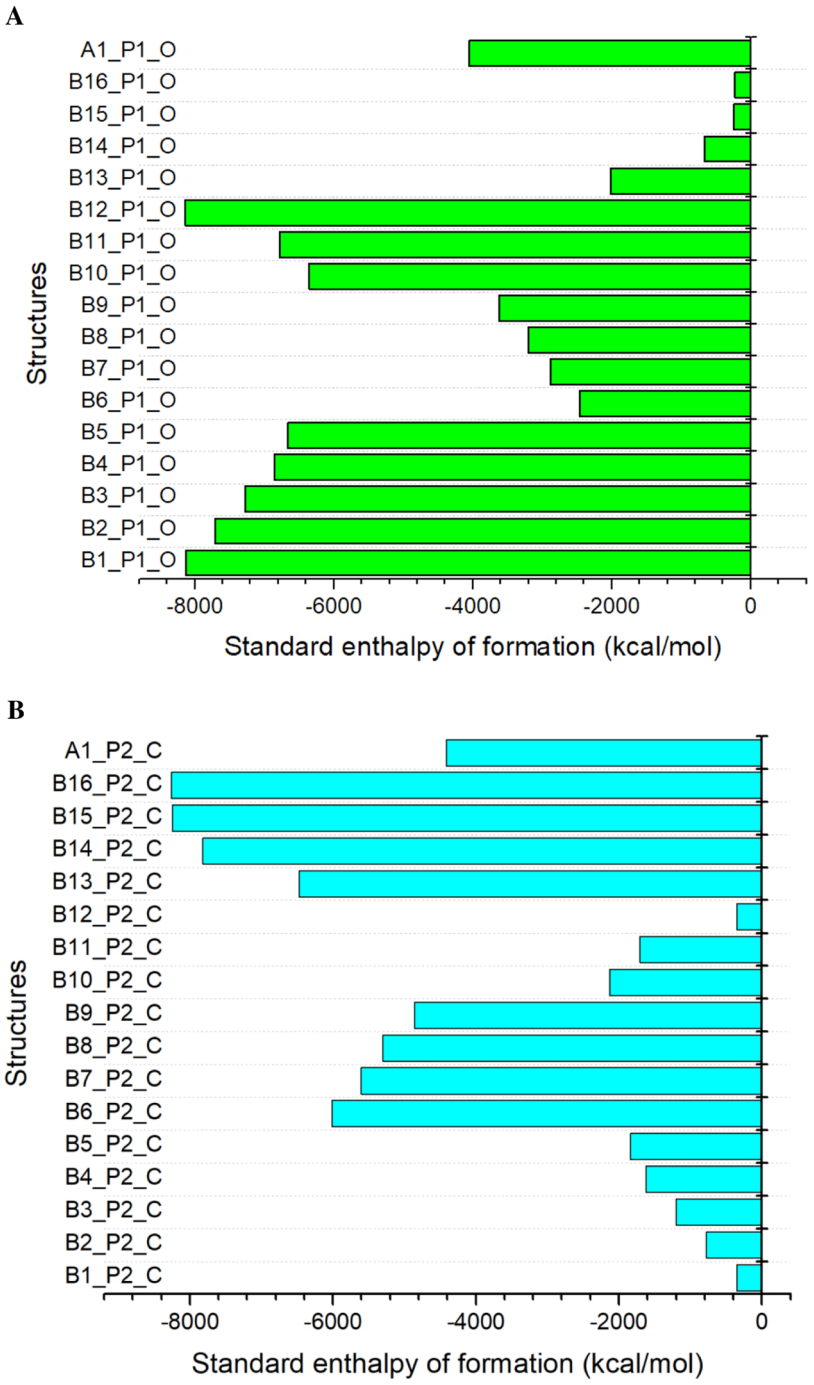

Figure 6. (A) Standard enthalpy of formation for product 1 species. (B) Standard enthalpy of formation for product 2 species.

those papers, we studied simplified linear lignin model oligomers, both of which had only one end-to-end distance to measure. In contrast, we studied a branched lignin polymer model in this work. Owing to the presence of one branch point arising from the 4-O-5 linkage, this structure has three different end-to-end distances that can be measured. All of these end-to-end distances varied irregularly during conformational sampling, thus making it impossible to use as the descriptor for the lowest energy conformer.

Bond Dissociation Enthalpies. Figure 4 depicts the value of BDEs from our calculation at 298.15 K for all of the pathways we considered in this work. All of the ether linkages were cleaved through homolysis resulting in two types of product species, phenoxy radicals as the product 1 species and carbon atom-centered radicals as the product 2 species.

We observed marked differences in our computed bond dissociation enthalpies along all of the pathways in this system. These differences in BDEs can be discussed in the context of the role of the neighboring groups, which was a major objective for performing this study (shown in Table 3).

Among the 16 pathways involving β-O-4 bond cleavage, eight pathways have two S units (S−S) as their neighbors. The average BDE for these eight pathways was calculated as 69.46 kcal mol^{-1}. β-O-4 bonds along seven pathways in our system have mixed neighbors, i.e., one G and one S unit (G−S) in four pathways with an average BDE of 58.56 kcal mol^{-1}, and one S

https://doi.org/10.1021/acs.energyfuels.2c03025
Energy Fuels XXXX, XXX, XXX−XXX

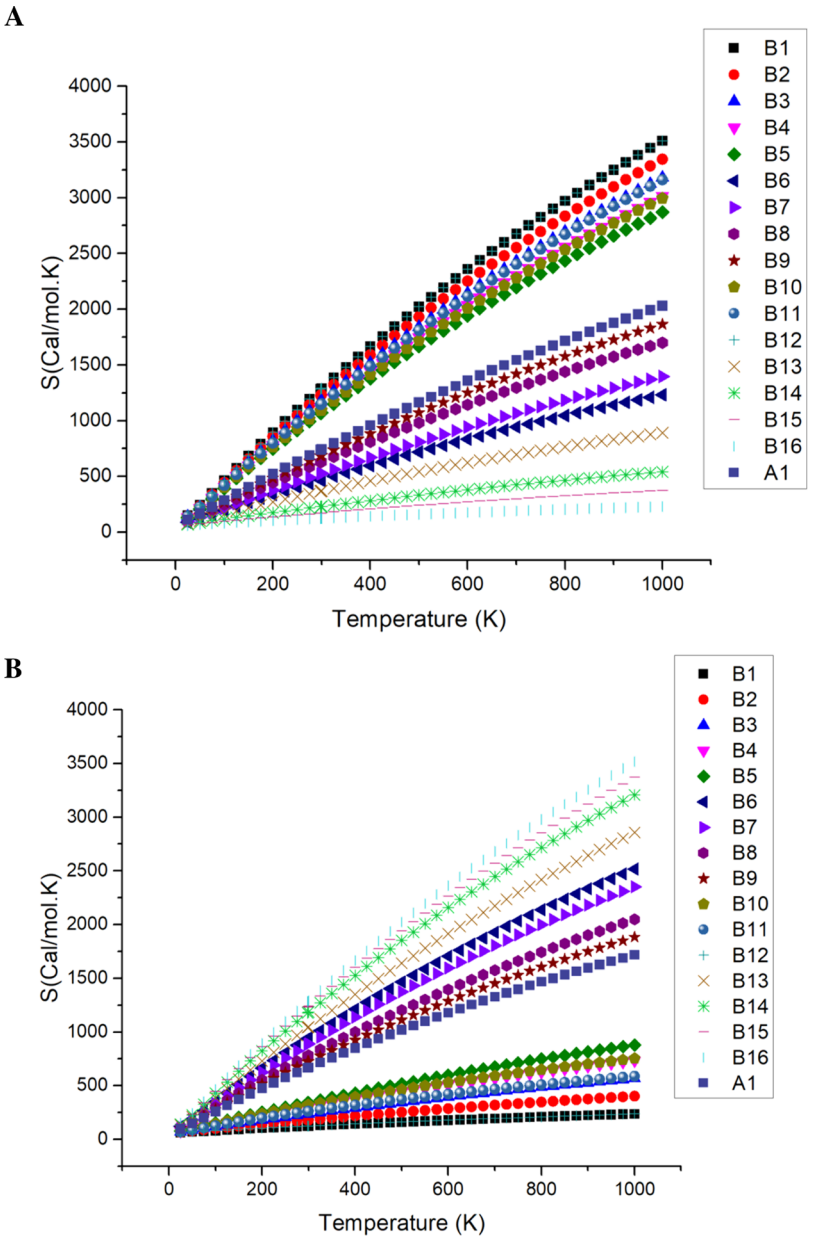

Figure 7. (A) Entropies of product 1 species. (B) Entropies of product 2 species.

and one G unit (S−G) in three pathways with an average BDE of 65.16 kcal mol^{-1}. There is only one pathway where the β-O-4 bond has two G units (G−G) as its neighbor with the BDE of 64.73 kcal mol^{-1}. Thus, a trend for BDE has been found from these observations, which is

$$BDE_{S-S} > BDE_{S-G} > BDE_{G-G} > BDE_{G-S}$$

It should be noted that the observed trend for BDE variation with the neighboring group has been found after inspecting only one optimized geometry of the 20-mer lignin model as the reactant and the radical products obtained from it. However, the observance of this effect might not be universal. Therefore, electronic structure analysis with multiple lignin models with a different order for the linkages and unit connections is necessary to check this effect in more detail.

Three factors might contribute to this observed neighboring effect in this work, including the nature of substituents in the aromatic rings, the position of the β-O-4 bonds, the lignin model, and the final conformation of the reactant molecule from which all of the product species were obtained. The difference in S and G unit monomer's substituents is that the S unit monomer consists of two methoxy groups ortho to the phenolic hydroxyl group, while the G unit monomer has only one such group at the ortho position. This difference in the amount of electron-donating groups present in the rings may play a significant role in the calculated BDEs. We also found a position dependence of the BDEs for the homolytic cleavage of β-O-4 bonds within the polymer chain. Cleaving β-O-4 bonds at the different positions resulted in product species of different molecular weights and nonbonded interactions, which can affect the BDEs. Finally, the observed trend of position dependence in the calculated BDEs can largely be attributed to the final conformation of the reactant molecule and the product species resulting from it. We did not study multiple lowest energy conformers for the species of this study with DFT methods to calculate BDEs. Nonetheless, the calculated

https://doi.org/10.1021/acs.energyfuels.2c03025
Energy Fuels XXXX, XXX, XXX−XXX

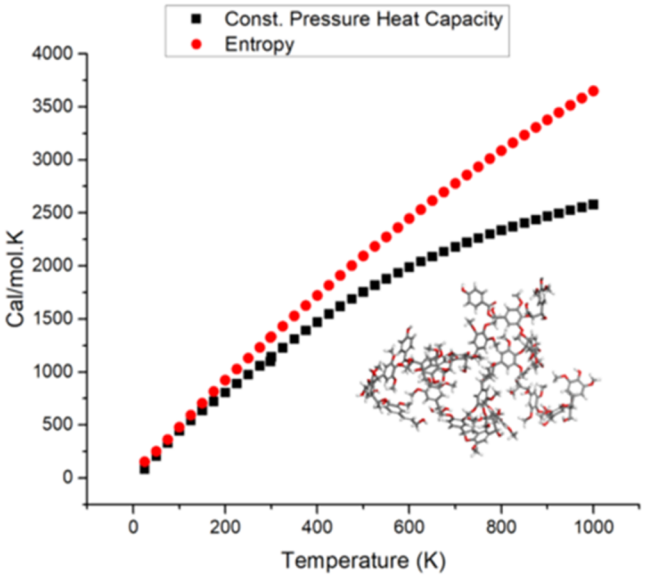

Figure 8. Standard thermodynamic properties (i.e., C_p and S) of the reactant molecule.

BDEs and the observed trend for its variation serve as an insight for native lignin pyrolysis responses.

In our previous study with a hardwood model lignin oligomer, we calculated the BDEs for the homolysis of nine β-O-4 bonds, all of which had two S unit monomers (S−S) as their neighbors. Despite the identical neighbors on each side of the bond, the range of calculated BDEs at the reference temperature for all nine pathways was 27.16 kcal mol^{-1}. Similarly, in our study with the softwood model lignin oligomer, all nine β-O-4 bonds had two G unit monomers (G−G) as their neighbors. We found a range of 19.5 kcal mol^{-1} in our calculated BDEs at the reference temperature with this softwood lignin model. This difference can be attributed to the different amount of nonbonded interactions arising from the different conformers of radical species as the products and also neighbor groups consisting of different substituents. Since the S−S neighbor group has more electron-donating substituents than the G−G neighbor group, the range of calculated BDEs using the hardwood model made of all S units was found to be higher than that for the softwood model made of all G units. Because we used a modified approach of conformational sampling from our previous works, the effect of conformational sampling has been captured differently. Our calculations from this study suggest that a smaller range of BDEs has been found at 298 K for all pathways, with a range of 11.58 kcal mol^{-1}, which is lower than the ranges previously observed. The similar stability of the formed product radical species might result in this small range of BDEs computed in this study.

Our results also indicate that the molecular weight of product species played a role in the BDE calculations for this study. The role of molecular weight also implies the role of nonbonded interactions for these product species. The BDEs are higher for four pathways, i.e., B_1 = 70.00 kcal mol^{-1}, B_3 = 72.16 kcal mol^{-1}, and B_4 = 71.04 kcal mol^{-1}, in which the product 1 species are larger than the product 2 species. The remainder of the reactions can be divided into three groups, namely, B_5, B_7−B_8, and B_9−B_{16}. Except for B_6, BDEs for the pathways B_5−B_{13} are relatively lower (average BDE is 61.32 kcal mol^{-1}). Both of the product species are somewhat similar in their molecular weights. Our results indicate that homolysis of β-O-4 bonds requires lower enthalpy when two products are similar in molecular weights. The reason for observing a higher BDE in pathway B_6 can be attributed to its neighboring group (S−S) and the conformation of the two product structures along this pathway. We anticipated observing higher BDE at the end of our lignin polymer model, i.e., along pathways B_{14}−B_{16} and B_{11}−B_{12}. However, we found BDEs lower than 70 kcal mol^{-1} along these five pathways (B_{14} = 69.08 kcal mol^{-1}, B_{15} = 65.84 kcal mol^{-1}, B_{16} = 64.73 kcal mol^{-1}, B_{11} = 66.63 kcal mol^{-1}, and B_{12} = 65.07 kcal mol^{-1}). This can be explained by the position of the β-O-4 bonds along these five pathways, which are near the tail of the polymer chain, closer to the branch point caused by the 4-O-5 linkage. We found a more dominant role of conformation of the reactant molecule, which was used to obtain the product species for these five pathways, than the other two factors, namely, the role of substituents and the molecular weights of the products. However, it was beyond the scope of this study to verify the predicted BDEs for these five pathways with a simpler model without a branch point. A truncated model with a 4-O-5 linkage and a 20-mer model without a 4-O-5 linkage could be used to investigate how the presence of branching caused by the 4-O-5 linkage affects the BDE calculation for a more realistic molecular model for lignin.

It is difficult to benchmark the BDE calculation for the homolysis of the C−O bond present in the β-O-4 linkage for lignin with experimental findings. The experimental BDEs are available only for simple and low MW ether molecules. For example, there are experimentally obtained BDEs for C−O present in alkyl ethers, roughly 80−84 kcal mol^{-1}, whereas such a value is not available for aryl ethers. The repeating units of the 20-mer model used in our current study include syringol and guaiacol-derived units. Diphenyl ether and phenyl benzyl ether are the structures closest to these repeating units. BDEs for these aryl ethers have been obtained experimentally as 52.1 and 79.4 kcal mol^{-1}, respectively.[72] Therefore, comparing our predicted BDEs with the available theoretical studies using similar structures is essential.[24,25,30,73,74]

One of the objectives of this work was to compare the BDEs with the other models used in contemporary theoretical studies. In addition to the difference in functionals and basis sets used in DFT methods, various structures have been investigated to calculate these BDEs, ranging from dimer to decamer. Table 4 compares our predicted BDEs for the homolysis of C−O at each pathway studied in this work with two seminal research articles on the theoretical BDE calculations using lignin model compounds.[22,23] While the levels of theory used in these two studies were different, i.e., MO6-2X/6-31G(d)//MO6-2X/6-311++G(d,p) in a study by Kim et al.[23] and MO6-2X/6-311++G(d,p) in a study by Parthasarathi et al.,[22] the BDEs reported in Table 4 were obtained for the same lignin structures as ours to calculate the BDEs of interest. Therefore, we compared our predicted BDEs with these two studies for each pathway. For three pathways, i.e., β5, β7, and β8, the percentage deviations from our predicted BDEs were higher. It should be noted that both Kim et al. and Parthasarathi et al. studied the BDEs of β-O-4 linkages with the model lignin dimers. On the contrary, we studied a very large model lignin oligomer where the final conformation of the species is influential in our BDE calculations. This is more important for pathways where the MWs of two products are similar, indicating similar non-bonded interactions on both radical species. It is noteworthy

https://doi.org/10.1021/acs.energyfuels.2c03025
Energy Fuels XXXX, XXX, XXX−XXX

that the overall mean BDE calculated in this study agrees with the other reported studies employing different levels of theories and also with the mean BDEs from the oligomer model studies using BLYP/DNP. This answers our query that the quantification of BDEs using the simpler models in the previous studies and the more realistic lignin model polymer is similar.

Standard Thermodynamic Properties. *Constant Pressure Heat Capacity.* We plotted our predicted constant pressure heat capacity (C_p) values as a function of temperature in Figure 5A,B for product 1 and 2 species, respectively. The smallest species in product 1 is a phenoxy radical with a molecular weight of 179 g mol^{-1}, whereas the smallest product 2 species has 227 g mol^{-1} as its molecular weight. Over the range of temperature 25−1000 K, we predicted a range of 10.12−108.95 and 11.25−130.27 cal mol^{-1} K^{-1} for these two species, respectively. The largest phenoxy radical we studied in this work has a MW of 4283 g mol^{-1} for which our predicted range of C_p is 79.62−2450.79 cal mol^{-1} K^{-1}. At the same temperature range, we predicted a range of C_p of 80.75−2472.11 cal mol^{-1} K^{-1} for the largest product 2 species with a MW of 4331 g mol^{-1}. Along with temperature, we found that the C_p values are related to the molecular weights for both types of radical species. This dependence on MW of C_p values has been both qualitatively and quantitatively depicted in Figure 5. Four clusters of phenoxy radicals arising from differences in MWs, i.e., radicals for pathways B_1−B_5; A_1, B_8−B_9; B_6−B_7; and B_{13}−B_{16}, can be seen in Figure 5A. Similarly, we found three clusters of radical species of product 2 in Figure 5B, namely, radicals for pathways B_{14}−B_{16}; B_6−B_9; A_1, B_1−B_5; and B_{11}−B_{12}. We calculated the range of C_p values for the 20-mer reactant closed shell molecule as 83.78−2578.82 cal mol^{-1} K^{-1}. In Table 5, we compared our predicted C_p values from this work with experimentally obtained quantifications for lignin models using different extraction methods at three different temperatures.

Standard Enthalpy of Formation. We used the atomization energy method for the calculation of enthalpy of formation, which requires the ab initio calculated enthalpy of atomization at 298 K and the experimental standard enthalpy of formation of atoms in the gas phase at the same temperature. Our prediction for the enthalpy of formation for the native hardwood model lignin polymer was −8553.7956 kcal mol^{-1}. The range of enthalpy of formation values predicted for phenoxy radical products is (−228.64 kcal mol^{-1}) − (−8139.72 kcal mol^{-1}). A similar range of variation, i.e., (−349.01 kcal mol^{-1}) − (−8260.43 kcal mol^{-1}), has been obtained for the carbon-free radical species of varying sizes. Figure 6A,B plots our prediction for standard enthalpies of formation for phenoxy and carbon-centered radical species, respectively.

Entropy. The variation of standard entropy for all species of both radical types has been plotted as a function of temperature in Figure 7A,B. Similar to our predictions for C_p values, our predicted entropy values also show a strong dependence on MW along with the temperature. The range of calculated entropy values for the smallest product 1 species (MW = 179 g mol^{-1}) was 60.66−229.56 cal mol^{-1} K^{-1}, whereas the range obtained for the largest species in this category (MW = 4283 g mol^{-1}) was 149.56−3511.513 cal mol^{-1} K^{-1}. Species of product 2 also showed a similar range of entropies over the same temperature range of 25−1000 K. Similar to the clusters of radicals observed in the plots of C_p as a function of temperature and different MWs, different clusters can be identified in Figure 7A,B. In these two figures, predicted entropies of the radicals that were obtained after the homolysis of β-O-4 along five pathways, namely, B_1−B_5, showed marked clustering. This is due to the structural similarity coming from the successive addition of one S unit in each monomer for the radicals along these five pathways. Our calculated range of entropy for the 20-mer reactant molecule is 154.32−3650.19 cal mol^{-1} K^{-1} over the temperature range of 25−1000 K.

Our predicted values of C_p and entropy for the 20-mer reactant molecule of native lignin over the range of temperature 25−1000 K have been shown in Figure 8.

CONCLUSIONS

Based on the insights from a previously reported experimental investigation, we modeled a lignin polymer consisting of twenty repeating units in the current work to study reaction energetics of initial stages in lignin pyrolysis following the radical mechanism. The presence of multiple linkages and monolignols made this molecular model a more realistic model of native hardwood lignin. The radical mechanism was followed in this work with the determination of bond dissociation enthalpies for all 16 β-O-4 linkages present in this 20-mer lignin model. We predicted a range of BDEs for the homolysis of β-O-4 over a wide range of temperatures, which can serve to compare the activation barrier for other competitive pathways. The larger model studied in this work allowed us to investigate the role of more realistic nonbonded interactions, which would be closer to native lignin. Using this very large lignin model, we followed the radical mechanism to study the reaction energetics relevant to its pyrolysis conditions. However, using the same model structure for studying reaction energetics of lignin pyrolysis following the concerted mechanism could help to reach a conclusion about which mechanism is more favorable for lignin decomposition. Prior to evaluating reaction energetics with DFT calculations, the conformational search method using the COMPASS forcefield (developed and used in previous studies) was used to identify the lowest energy conformers for the closed shell 20-mer reactant molecule in the current work. We observed a trend of the neighboring effect arising from the presence of various monolignols in our calculated BDEs with the lignin model polymer used in our current study. However, it is beyond the scope of this study to verify if this neighboring effect is a global phenomenon for such more realistic lignin models. We recommend studying several 20-mer models altering the monomer and linkage order within the polymer chain and applying machine learning tools to investigate it. This molecular model was generated based on experimental evidence, unlike the previous models that have been used in similar studies using simple lignin model compounds. Our results show that the range of BDEs computed in the reference temperature in this work is similar to the predicted BDEs obtained with simple models in previous works. The difficulty in making a comparison between BDE results obtained with different computational methods and models should also be considered. Nonetheless, further theoretical calculations with different methods for dispersion correction could be helpful in verifying this similarity in the calculated BDEs. Overall, this study adds novel insights to our systematic quest for computational investigation of the gas-phase reaction energetics of primary lignin pyrolysis with a more realistic 20-mer lignin model. The predicted reaction enthalpies and the

https://doi.org/10.1021/acs.energyfuels.2c03025
Energy Fuels XXXX, XXX, XXX−XXX

standard thermodynamic properties would be particularly useful for constructing a complex and detailed reaction network for lignin pyrolysis, reactor design, and process optimization dedicated to lignin valorization.

■ ASSOCIATED CONTENT

Supporting Information

The Supporting Information is available free of charge at https://pubs.acs.org/doi/10.1021/acs.energyfuels.2c03025.

Computational methodology (extended); molecular weights of all species studied in this work (Table S1); variation of thermodynamic properties with temperature for the 22-mer reactant structure: heat capacity, entropy, and standard Gibbs free energy (Table S2); variation of reaction enthalpy for the homolytic cleavage of β-O-4 bonds in the primary pyrolysis temperature range (Figure S1); variation of standard Gibbs free energy of formation with temperature for product 1 species (Figure S2); variation of standard Gibbs free energy of formation with temperature for product 2 species (Figure S3); standard Gibbs free energy of formation as a function of temperature for the 22-mer structure (Figure S4) (PDF)

■ AUTHOR INFORMATION

Corresponding Author

Andrew J. Adamczyk − *Department of Chemical Engineering, Auburn University, Auburn, Alabama 36849, United States;* orcid.org/0000-0002-9523-7849; Email: aja0056@auburn.edu

Authors

Tanzina Azad − *Department of Chemical Engineering, Auburn University, Auburn, Alabama 36849, United States*

Maria L. Auad − *Department of Chemical Engineering, Auburn University, Auburn, Alabama 36849, United States; Center for Polymer and Advanced Composites, Auburn, Alabama 36849, United States;* orcid.org/0000-0001-6932-5645

Thomas Elder − *United States Department of Agriculture (USDA) Forest Service, Southern Research Station, Auburn, Alabama 36849, United States;* orcid.org/0000-0003-3909-2152

Complete contact information is available at: https://pubs.acs.org/10.1021/acs.energyfuels.2c03025

Notes

The authors declare no competing financial interest.

■ ACKNOWLEDGMENTS

The authors are grateful for support of this work by the Alabama Supercomputing Center, Auburn University Hopper and Easley high-performance compute cluster resources, USDA grant 18-JV-11330131-073 and Auburn University new faculty start-up funding.

■ REFERENCES

(1) Boerjan, W.; Ralph, J.; Baucher, M. Lignin biosynthesis. *Annu. Rev. Plant Biol.* **2003**, *54*, 519−546.

(2) Sticklen, M. B. Plant genetic engineering for biofuel production: towards affordable cellulosic ethanol (Retraction of vol 9, pg 433, 2008). *Nat. Rev. Genet.* **2010**, *11*, 308.

(3) Weng, J. K.; Li, X.; Bonawitz, N. D.; Chapple, C. Emerging strategies of lignin engineering and degradation for cellulosic biofuel production. *Curr. Opin. Biotechnol.* **2008**, *19*, 166−172.

(4) Mansfield, S. D. Solutions for dissolution-engineering cell walls for deconstruction. *Curr. Opin. Biotechnol.* **2009**, *20*, 286−294.

(5) Rinaldi, R.; Tandem, A. for Lignin-First Biorefinery. *Joule* **2017**, *1*, 427−428.

(6) Kumar, A.; Jindal, M.; Maharana, S.; Thallada, B. Lignin Biorefinery: New Horizons in Catalytic Hydrodeoxygenation for the Production of Chemicals. *Energy Fuels* **2021**, *35*, 16965−16994.

(7) Liu, Z. H.; Hao, N. J.; Wang, Y. Y.; Dou, C.; Lin, F. R.; Shen, R. C.; Bura, R.; Hodge, D. B.; Dale, B. E.; Ragauskas, A. J.; Yang, B.; Yuan, J. S. Transforming biorefinery designs with 'Plug-In Processes of Lignin' to enable economic waste valorization. *Nat. Commun.* **2021**, *12*, No. 3912.

(8) Yao, L.; Yang, H. T.; Meng, X. Z.; Ragauskas, A. J. Toward a Fundamental Understanding of the Role of Lignin in the Biorefinery Process. *Front. Energy Res.* **2022**, *9*, 804086.

(9) Schultz, T. P.; Templeton, M. C. Proposed Mechanism For The Nitrobenzene Oxidation Of Lignin. *Holzforschung* **1986**, *40*, 93−97.

(10) Haz, A. J. M.; Orsagova, A.; Surina, I. In *Characterization of Lignins by Py/GC/MS*, 4th International Scientific Conference OZE Renewable Energy Sources, Slovak Republic, 2013.

(11) Lapierre, C.; Monties, B.; Rolando, C.; Chirale, L. Thioacidolysis of lignin - Comparison with acidolysis. *J. Wood Chem. Technol.* **1985**, *5*, 277−292.

(12) Lu, F. C.; Ralph, J. Derivatization followed by reductive cleavage (DFRC method), a new method for lignin analysis: Protocol for analysis of DFRC monomers. *J. Agric. Food Chem.* **1997**, *45*, 2590−2592.

(13) Vanholme, R.; Demedts, B.; Morreel, K.; Ralph, J.; Boerjan, W. Lignin Biosynthesis and Structure. *Plant Physiol.* **2010**, *153*, 895−905.

(14) Vasile, C.; Gosselink, R.; Quintas, P.; Koukios, E. G.; Koullas, D. P.; Avgerinos, E.; Abacherli, D. A. Analytical methods for lignin characterization. I. Thermogravimetry. *Cell Chem. Technol.* **2006**, *40*, 421−429.

(15) Popescu, C. M.; Vasile, C.; Popescu, M. C.; Singurec, G.; Popa, V. I.; Munteanu, B. S. Analytical methods for lignin characterization. II. Spectroscopic studies. *Cell Chem. Technol.* **2006**, *40*, 597−621.

(16) Stewart, J. J.; Akiyama, T.; Chapple, C.; Ralph, J.; Mansfield, S. D. The Effects on Lignin Structure of Overexpression of Ferulate 5-Hydroxylase in Hybrid Poplar. *Plant Physiol.* **2009**, *150*, 621−635.

(17) Ralph, J.; Lapierre, C.; Boerjan, W. Lignin structure and its engineering. *Curr. Opin. Biotechnol.* **2019**, *56*, 240−249.

(18) Crestini, C.; Melone, F.; Sette, M.; Saladino, R. Milled Wood Lignin: A Linear Oligomer. *Biomacromolecules* **2011**, *12*, 3928−3935.

(19) Ralph, J.; Brunow, G.; Boerjan, W.Lignins. In *Encyclopedia of Life Sciences*; Wiley: Chichester, UK, 2007.

(20) Fernando, S.; Adhikari, S.; Chandrapal, C.; Murali, N. Biorefineries: Current status, challenges, and future direction. *Energy Fuels* **2006**, *20*, 1727−1737.

(21) Elder, T.; del Rio, J. C.; Ralph, J.; Rencoret, J.; Kim, H.; Beckham, G. T. Radical coupling reactions of piceatannol and monolignols: A density functional theory study. *Phytochemistry* **2019**, *164*, 12−23.

(22) Parthasarathi, R.; Romero, R. A.; Redondo, A.; Gnanakaran, S. Theoretical Study of the Remarkably Diverse Linkages in Lignin. *J. Phys. Chem. Lett.* **2011**, *2*, 2660−2666.

(23) Kim, S.; Chmely, S. C.; Nimos, M. R.; Bomble, Y. J.; Foust, T. D.; Paton, R. S.; Beckham, G. T. Computational Study of Bond Dissociation Enthalpies for a Large Range of Native and Modified Lignins. *J. Phys. Chem. Lett.* **2011**, *2*, 2846−2852.

(24) Elder, T. Bond Dissociation Enthalpies of a Dibenzodioxocin Lignin Model Compound. *Energy Fuels* **2013**, *27*, 4785−4790.

(25) Elder, T. Bond Dissociation Enthalpies of a Pinoresinol Lignin Model Compound. *Energy Fuels* **2014**, *28*, 1175−1182.

(26) Elder, T.; Beste, A. Density Functional Theory Study of the Concerted Pyrolysis Mechanism for Lignin Models. *Energy Fuels* **2014**, *28*, 5229−5235.

(27) Shen, Q. R.; Fu, Z. W.; Li, R.; Wu, Y. L. A study on the pyrolysis mechanism of a beta-O-4 lignin dimer model compound using DFT combined with Py-GC/MS. *J. Therm. Anal. Calorim.* **2021**, *146*, 1751−1761.
(28) Li, S. M.; Luo, Z. Y.; Wang, W. B.; Lu, K. Y.; Yang, Y.; Liang, X. R. Characterization of pyrolytic lignin and insight into its formation mechanisms using novel techniques and DFT method. *Fuel* **2020**, *262*, 116516.
(29) Jiang, W. K.; Wu, S. B. Mechanism Study on Depolymerization of the alpha-O-4 Linkage Lignin Model Compound in Supercritical Ethanol System. *Waste Biomass Valorization* **2019**, *10*, 197−204.
(30) Houston, R. W.; Elder, T. J.; Abdoulmoumine, N. H. Investigation into the Pyrolysis Bond Dissociation Enthalpies (BDEs) of a Model Lignin Oligomer Using Density Functional Theory (DFT). *Energy Fuels* **2022**, *36*, 1565−1573.
(31) Klein, M. T.; Virk, P. S. Model Pathways In Lignin Thermolysis. 1. Phenethyl Phenyl Ether. *Ind. Eng. Chem. Fundam.* **1983**, *22*, 35−45.
(32) Jarvis, M. W.; Daily, J. W.; Carstensen, H. H.; Dean, A. M.; Sharma, S.; Dayton, D. C.; Robichaud, D. J.; Nimlos, M. R. Direct Detection of Products from the Pyrolysis of 2-Phenethyl Phenyl Ether. *J. Phys. Chem. A* **2011**, *115*, 428−438.
(33) Britt, P. F.; Buchanan, A. C.; Malcolm, E. A. Thermolysis Of Phenethyl Phenyl Ether - A Model For Ether Linkages In Lignin And Low-rank Coal. *J. Org. Chem.* **1995**, *60*, 6523−6536.
(34) Britt, P. F.; Buchanan, A. C.; Cooney, M. J.; Martineau, D. R. Flash vacuum pyrolysis of methoxy-substituted lignin model compounds. *J. Org. Chem.* **2000**, *65*, 1376−1389.
(35) Kishimoto, T.; Sano, Y. Delignification mechanism during high-boiling solvent pulping - Part 2. Homolysis of guaiacylglycerol-beta-guaiacyl ether. *Holzforschung* **2002**, *56*, 623−631.
(36) Li, S.; Lundquist, K. Reactions of the beta-aryl ether lignin model 1-(4-hydroxy-3-methoxyphenyl)-2-(2-methoxyphenoxy)-1-propanol on heating in aqueous solution. *Holzforschung* **2001**, *55*, 296−301.
(37) Tanahashi, M.; Karina, M.; Tamabuchi, K.; Higuchi, T. Degradation Mechanism Of Lignin Accompanying Steam Explosions. 1. Degradation Products Of Lignin And Beta-O-4 Lignin Substructure Model Dimers. *Mokuzai Gakkaishi* **1989**, *35*, 135−143.
(38) Azad, T.; Schuler, J. D.; Auad, M. L.; Elder, T.; Adamczyk, A. J. Model Lignin Oligomer Pyrolysis: Coupled Conformational and Thermodynamic Analysis of beta-O-4 ' Bond Cleavage. *Energy Fuels* **2020**, *34*, 9709−9724.
(39) Azad, T.; Torres, H. F.; Auad, M. L.; Elder, T.; Adamczyk, A. J. Isolating key reaction energetics and thermodynamic properties during hardwood model lignin pyrolysis. *Phys. Chem. Chem. Phys.* **2021**, *23*, 20919−20935.
(40) Adler, E. Lignin Chemistry - Past, Present And Future. *Wood Sci. Technol.* **1977**, *11*, 169−218.
(41) Lu, F. C.; Ralph, J.; Morreel, K.; Messens, E.; Boerjan, W. Preparation and relevance of a cross-coupling product between sinapyl alcohol and sinapyl p-hydroxybenzoate. *Org. Biomol. Chem.* **2004**, *2*, 2888−2890.
(42) Sun, H. COMPASS: An ab initio force-field optimized for condensed-phase applications - Overview with details on alkane and benzene compounds. *J. Phys. Chem. B* **1998**, *102*, 7338−7364.
(43) Metropolis, N.; Rosenbluth, A. W.; Rosenbluth, M. N.; Teller, A. H.; Teller, E. Equation Of State Calculations By Fast Computing Machines. *J. Chem. Phys.* **1953**, *21*, 1087−1092.
(44) Gill, P. M. W.; Johnson, B. G.; Pople, J. A.; Frisch, M. J. The Performance Of The Becke-lee-yang-parr (B-lyp) Density Functional Theory With Various Basis-sets. *Chem. Phys. Lett.* **1992**, *197*, 499−505.
(45) Deng, S. D.; Du, G. B.; Li, X. H.; Xie, X. G. Performance, Reaction Mechanism, and Characterization of Glyoxal-Monomethylol Urea (G-MMU) Resin. *Ind. Eng. Chem. Res.* **2014**, *53*, 5421−5431.
(46) Tan, B. S.; Peng, R. F.; Li, H. B.; Jin, B.; Chu, S. J.; Long, X. P. Theoretical Investigation of an Energetic Fullerene Derivative. *J. Comput. Chem.* **2010**, *31*, 2233−2237.
(47) Wang, J. Q.; Liu, L. L.; Wilson, A. K. Oxidative Cleavage of the beta-O-4 Linkage of Lignin by Transition Metals: Catalytic Properties and the Performance of Density Functionals. *J. Phys. Chem. A* **2016**, *120*, 737−746.
(48) van Mourik, T.; Danilov, V. I.; Dailidonis, V. V.; Kurita, N.; Wakabayashi, H.; Tsukamoto, T. A DFT study of uracil and 5-bromouracil in nanodroplets. *Theor. Chem. Acc.* **2010**, *125*, 233−244.
(49) Tkatchenko, A.; Scheffler, M. Accurate Molecular Van Der Waals Interactions from Ground-State Electron Density and Free-Atom Reference Data. *Phys. Rev. Lett.* **2009**, *102*, 073005.
(50) McQuarrie, D. A. Statistical Mechanics. *Phys. Today* **1965**, *18*, 74−75.
(51) Adamczyk, A. J.; Broadbelt, L. J. Thermochemical Property Estimation of Hydrogenated Silicon Clusters. *J. Phys. Chem. A* **2011**, *115*, 8969−8982.
(52) Adamczyk, A. J.; Reyniers, M. F.; Marin, G. B.; Broadbelt, L. J. Exploring 1,2-Hydrogen Shift in Silicon Nanoparticles: Reaction Kinetics from Quantum Chemical Calculations and Derivation of Transition State Group Additivity Database. *J. Phys. Chem. A* **2009**, *113*, 10933−10946.
(53) Adamczyk, A. J.; Reyniers, M. F.; Marin, G. B.; Broadbelt, L. J. Kinetics of Substituted Silylene Addition and Elimination in Silicon Nanocluster Growth Captured by Group Additivity. *ChemPhysChem* **2010**, *11*, 1978−1994.
(54) Adamczyk, A. J.; Reyniers, M. F.; Marin, G. B.; Broadbelt, L. J. Kinetic correlations for H-2 addition and elimination reaction mechanisms during silicon hydride pyrolysis. *Phys. Chem. Chem. Phys.* **2010**, *12*, 12676−12696.
(55) Adamczyk, A. J.; Broadbelt, L. J. The Role of Multifunctional Kinetics during Early-Stage Silicon Hydride Pyrolysis: Reactivity of Si2H2 Isomers with SiH4 and Si2H6. *J. Phys. Chem. A* **2011**, *115*, 2409−2422.
(56) Choi, Y.; Adamczyk, A. J. Competitive Hydrogen Migration in Silicon Nitride Nanoclusters:Reaction Kinetics Generalized from Supervised Machine Learning. *J. Phys. Chem. A* **2022**, *126*, 2677−2689.
(57) Lawson, K. E.; Dekle, J. K.; Evans, M. N.; Adamczyk, A. J. Deamidation reaction network mapping of pharmacologic and related proteins: impact of solvation dielectric on the degradation energetics of asparagine dipeptides. *React. Chem. Eng.* **2022**, *7*, 1525−1543.
(58) Choi, Y.; Preston, T. J.; Adamczyk, A. J. Data-Driven Investigation of Monosilane and Ammonia Co-Pyrolysis to Silicon-Nitride-Based Ceramic Nanomaterials. *ChemPhysChem* **2020**, *21*, 2627−2642.
(59) Lozano-Blanco, G.; Adamczyk, A. J. Cobalt-catalyzed nitrile hydrogenation: Insights into the reaction mechanism and product selectivity from DFT analysis. *Surf. Sci.* **2019**, *688*, 31−44.
(60) Lozano-Blanco, G.; Tatarchuk, B. J.; Adamczyk, A. J. Building a Microkinetic Model from First Principles for Higher Amine Synthesis on Pd Catalyst. *Ind. Eng. Chem. Res.* **2019**, *58*, 19022−19032.
(61) Minkler, M. J.; Kim, J.; Lawson, K. E.; Ali, A.; Zhao, R.; Adamczyk, A. J.; Beckingham, B. S. Solution processible statistical poly(3-methoxythiophene)-co-poly (3-hexylthiophene) copolymer. *Mater. Lett.* **2019**, *256*, 126563.
(62) Wu, S. Y.; Tatarchuk, B. J.; Adamczyk, A. J. Ethylene oxidation on unpromoted silver catalysts: Reaction pathway and selectivity analysis using DFT calculations. *Surf. Sci.* **2021**, *708*, 121834.
(63) Wang, Z.; Nautiyal, A.; Alexopoulos, C.; Aqrawi, R.; Huang, X. Z.; Ali, A.; Lawson, K. E.; Riley, K.; Adamczyk, A. J.; Dong, P.; Zhang, X. Y. Fentanyl Assay Derived from Intermolecular Interaction-Enabled Small Molecule Recognition (iMSR) with Differential Impedance Analysis for Point-of-Care Testing. *Anal. Chem.* **2022**, *94*, 9242−9251.
(64) Berstis, L.; Elder, T.; Crowley, M.; Beckham, G. T. Radical Nature of C-Lignin. *ACS Sustainable Chem. Eng.* **2016**, *4*, 5327−5335.
(65) Berstis, L.; Elder, T.; Dixon, R.; Crowley, M.; Beckham, G. T. Coupling of Flavonoid Initiation Sites with Monolignols Studied by Density Functional Theory. *ACS Sustainable Chem. Eng.* **2021**, *9*, 1518−1528.

https://doi.org/10.1021/acs.energyfuels.2c03025
Energy Fuels XXXX, XXX, XXX−XXX

(66) Karhunen, P.; Rummakko, P.; Sipila, J.; Brunow, G.; Kilpelainen, I. Dibenzodioxocins - A Novel Type Of Linkage In Softwood Lignins. *Tetrahedron Lett.* **1995**, *36*, 169−170.
(67) Lu, F. C.; Ralph, J. Detection and determination of p-coumaroylated units in lignins. *J. Agric. Food Chem.* **1999**, *47*, 1988−1992.
(68) Kilpelainen, I.; Sipila, J.; Brunow, G.; Lundquist, K.; Ede, R. M. Application Of 2-dimensional NMR-spectroscopy To Wood Lignin Structure Determination And Identification Of Some Minor Structural Units Of Hardwood And Softwood Lignins. *J. Agric. Food Chem.* **1994**, *42*, 2790−2794.
(69) Orella, M. J.; Gani, T. Z. H.; Vermaas, J. V.; Stone, M. L.; Anderson, E. M.; Beckham, G. T.; Brushett, F. R.; Roman-Leshkov, Y. Lignin-KMC: A Toolkit for Simulating Lignin Biosynthesis. *ACS Sustainable Chem. Eng.* **2019**, *7*, 18313−18322.
(70) Sangha, A. K.; Parks, J. M.; Standaert, R. F.; Ziebell, A.; Davis, M.; Smith, J. C. Radical Coupling Reactions in Lignin Synthesis: A Density Functional Theory Study. *J. Phys. Chem. B* **2012**, *116*, 4760−4768.
(71) Elder, T.; Berstis, L.; Beckham, G. T.; Crowley, M. F. Coupling and Reactions of 5-Hydroxyconiferyl Alcohol in Lignin Formation. *J. Agric. Food Chem.* **2016**, *64*, 4742−4750.
(72) Luo, Y.-R.*Handbook of Bond Dissociation Energies in Organic Compounds*; CRC Press LLC: Boca Raton, FL, 2003.
(73) Huang, J. B.; Liu, C.; Jin, Q. J.; Tong, H.; Li, W. M.; Wu, D. Density functional theory study on bond dissociation enthalpies for lignin dimer model compounds. *J. Renewable Sustainable Energy* **2014**, *6*, 033116.
(74) Zhang, J. J.; Jiang, X. Y.; Ye, X. N.; Chen, L.; Lu, Q.; Wang, X. H.; Dong, C. Q. Pyrolysis mechanism of a beta-O-4 type lignin dimer model compound. *J. Therm. Anal. Calorim.* **2016**, *123*, 501−510.
(75) Voitkevich, O. V.; Kabo, G. J.; Blokhin, A. V.; Paulechka, Y. U.; Shishonok, M. V. Thermodynamic Properties of Plant Biomass Components. Heat Capacity, Combustion Energy, and Gasification Equilibria of Lignin. *J. Chem. Eng. Data* **2012**, *57*, 1903−1909.
(76) Hatakeyama, T.; Nakamura, K.; Hatakeyama, H. Studies On Heat-Capacity Of Cellulose And Lignin By Differential Scanning Calorimetry. *Polymer* **1982**, *23*, 1801−1804.

https://doi.org/10.1021/acs.energyfuels.2c03025
Energy Fuels XXXX, XXX, XXX−XXX